Fully coupled nonlinear thermomechanical modeling of composites using mean-field Mori-Tanaka scheme combined with TFA theory

George Chatzigeorgiou[a,*], Fodil Meraghni[a], Qiang Chen[a]

[a] *Arts et Métiers Institute of Technology, CNRS, Université de Lorraine, LEM3 UMR CNRS 7239, F-57070 Metz, France*

Abstract

This article aims at proposing a new mean-field homogenization framework for the study of composites undergoing fully coupled thermomechanical processes. Strongly dissipative phenomena during high or moderate cyclic loading conditions in a structural component made of a composite material cause significant interplay between mechanical and thermal fields. The proposed framework attempts to address such effect by combining the Mori-Tanaka scheme and the Transformation Field Analysis (TFA) theory and by developing a multiscale framework capable of taking into account thermomechanically coupled processes. The numerical simulations performed in the examples section and validations with computations using periodic homogenization and full-structure analysis demonstrate the proposed strategy's accuracy and robustness. The numerical simulation of a tube shows the model's ability to simulate cyclic loading conditions with significantly less computa-

*Corresponding author.

Email addresses: georges.chatzigeorgiou@ensam.eu (George Chatzigeorgiou), fodil.meraghni@ensam.eu (Fodil Meraghni), qiangchen@xjtu.edu.cn (Qiang Chen)

tional cost than the alternative FE^2 computation strategies. This drastic computational time reduction is due to the semi-analytical formalism of the micromechanics methodology.

Keywords: Thermomechanical processes; Composites; Mori-Tanaka method; Transformation Field Analysis; Tangent operators.

1. Introduction

Many industries, such as the automotive and the aerospace, demand the design of novel material systems, usually composites, that can be adopted to complex and lightweight structures with high needs in strength, multi-functionality and durability. In addition, these structures are required to exhibit long lifetime during repeated loading cycles. Since the cyclic behavior is usually accompanied with dissipative mechanisms, it becomes of vital importance to develop innovative and smart computational tools, capable of predicting structural responses under coupled thermomechanical conditions.

Composite structures are frequently operating at regimes where highly dissipative phenomena occur, such as plasticity, viscoplasticity, viscoelasticity, damage, and/or phase transformation (Chatzigeorgiou et al., 2015, 2018, 2022). These phenomena are accompanied by dissipation which may lead to a significant temperature increase of the material. This in return impacts the mechanical response of the structural component, notably when it deals with polymer matrix composites. Considering the energy exchanges during thermomechanical loading cycles is a key factor on predicting accurately the fatigue behavior of composite media and structures (Chrysochoos et al., 2010; Benaarbia et al., 2015, 2019). Indeed, couplings of mechanical and thermal

fields have a particularly significant impact in semi-crystalline polymer based composites. The behavior of the latter can change drastically at temperature ranges above or below the glass transition temperature.

In homogeneous materials, strong thermomechanical couplings have been addressed from a modeling point of view by many authors. Thermodynamic frameworks combined with the concept of generalized standard materials (Germain, 1973; Halphen and Nguyen, 1975; Germain, 1982; Germain et al., 1983) have led to the development of advanced phenomenological models for dissipative materials. In composites, however, the scale transitions that exist between the microstructure and the overall structure create certain challenges in defining appropriate thermodynamics tools. Usually thermomechanical effects in heterogeneous media are taken into account through two ways: i) Similar to homogeneous media, by designing and implementing phenomenological type of models, accounting for possible anisotropy due to microstructure effects. ii) Through homogenization frameworks that take into account the thermomechanical processes.

The purely mechanical behavior of heterogeneous, nonlinear, dissipative composite materials has been extensively studied in the literature. A plethora of multiscale techniques have been proposed aiming at identifying the response of viscoelastic, elastoplastic, viscoplastic, or damaged composite structures.

Mori-Tanaka and self consistent schemes have been introduced for the identification of the viscoplastic response of random media (Mercier and Molinari, 2009). Mean-field and analytical methods in general are popular approaches for the analysis of various nonlinear behaviors and mecha-

nisms: viscoelastic (Vu et al., 2012; Brenner and Suquet, 2013; Schöneich et al., 2017), elastoplastic (Zecevic and Knezevic, 2018; Kotha et al., 2019), viscoplastic (Rao et al., 2019), damage (Desrumaux et al., 2001; Meraghni et al., 2002; Jendli et al., 2009), damage and plasticity (Yun et al., 2021). Mori-Tanaka scheme has also been used in peridynamics simulations of composites (Buryachenko, 2024). The mean-field based approaches like Mori-Tanaka and self consistent frequently produce stiff responses due to the lack of information on the inelastic strains. To address this issue, several authors have adopted the so-called isotropization method for eleastoplastic (Doghri and Ouaar, 2003; Chaboche et al., 2005; Jiang and Shao, 2009), viscoplastic (Czarnota et al., 2015) or viscoelastic-viscoplastic (Miled et al., 2013) composites. Based on the pivotal work of Ponte-Castañeda (1991), many authors have developed methodologies based on the concept of the linear comparison composite. The related works employ the variational-incremental approach (Lahellec and Suquet, 2007, 2013; Brassart et al., 2012; Boudet et al., 2016) or the incremental-secant approach (Wu et al., 2013, 2017), to study the elastoplastic and the viscoplastic response of composites.

Full-field homogenization schemes have been developed extensively for the study of composites with nonlinear behavior (Charalambakis et al., 2018). The finite element (FE) based periodic homogenization framework has been employed for analyzing the elastoplastic (Terada and Kikuchi, 2001; Asada and Ohno, 2007), viscoelastic, viscoplastic, damageable and combined (Praud et al., 2021; Tikarrouchine et al., 2021) nonlinear behavior of composites. Composites undergoing viscoplasticity coupled with damage have been analyzed through the combination of FE and Voronoi cells (Dondeti et al., 2012).

A popular numerical implementation of the periodic homogenization theory is through the Fast Fourier Transforms (FFT), proposed by Michel et al. (1999). This technique has been utilized in many recent studies (Schneider, 2017, 2021; Onimus et al., 2022), since it provides a faster alternative to the FE computations. Another methodology proposed in the literature is the so-called method of cells (Haj-Ali and Aboudi, 2010). The finite volume homogenization approach has been employed for the study of elastoplastic (Cavalcante and Pindera, 2016), viscoelastic (Chen et al., 2017; Chen and Pindera, 2020) and damage (Tu and Pindera, 2016) response of composites.

The Transformation Field Analysis, developed by Dvorak (1992); Dvorak and Benveniste (1992), has been proven to be a powerful tool for the analysis of composites. Combined with mean-field approaches has provided advanced models for the analysis of composites undergoing strongly nonlinear mechanisms, among them viscopasticity coupled with damage (Kruch and Chaboche, 2011) and viscoelasticity (Chen et al., 2022). TFA has also been combined with FE full-field computations in a representative volume element (RVE) (Alaimo et al., 2019). A modified version has been introduced by Michel and Suquet (2004), called nonuniform TFA (NTFA). The NTFA has been combined with full-field homogenization strategies in the case of viscoplastic (Covezzi et al., 2016) and elastoplastic (Ju et al., 2022) composites.

Concerning the fully coupled thermomechanical behavior, several multiscale strategies have been proposed quite recently, based on the periodic homogenization framework. In the earlier works, fully coupled thermomechanical processes by combining the conservations of linear momentum and

energy have been presented for elastic (Ene, 1983; Temizer, 2012) and viscoelastic (Yu and Fish, 2002) composites. Higher order theories have also been proposed in the literature for thermoelastic media (Dong et al., 2019; Yang et al., 2020). Using the zeroth order asymptotic expansion homogenization theory, Chatzigeorgiou et al. (2016) have established appropriate micromechanics framework for composites made of generalized standard materials. A computational scheme has also been introduced for the study of polycrystals (Li et al., 2019). In recent works, advanced thermomechanical homogenization numerical techniques have been developed, both using FE^2 (Sengupta et al., 2012; Berthelsen et al., 2017; Tikarrouchine et al., 2019) and FFT (Wicht et al., 2021).

The scope of this manuscript is to propose a mean-field based homogenization theory for the study of composite materials undergoing fully coupled thermomechanical processes. To the best of the authors knowledge, an attempt for such framework appeared only once in the literature (Chatzigeorgiou et al., 2018). However, the discussion there was limited to mostly theoretical development, and the mean-field methods were established using the tangent modulus approach. In this article, a combined Mori-Tanaka/TFA homogenization technique is discussed and explored.

The structure of the manuscript is as follows: Section 2 provides a brief recall of the homogenization theory for composites subjected to fully coupled thermomechanical conditions. Section 3 discusses the mean-field homogenization framework and its numerical implementation in finite element software. Section 4 presents three numerical examples that show the approach's robustness: the first two are used to validate the new multiscale model by

comparing its results towards more accurate strategies (periodic homogenization or full-structure analysis). The third example demonstrates the model's capabilities in a complex structural application. The main conclusions of the work and the potential perspectives are summarized in the corresponding section. An appendix regarding the normalization of the thermomechanical material parameters as a numerical hint is also included.

2. Theoretical background of thermomechanical homogenization framework

This section contains a summary of the fully coupled thermomechanical framework developed in Chatzigeorgiou et al. (2016) for generalized standard materials. The theoretical analysis in that contribution focuses on periodic media and is based on the asymptotic expansion periodic homogenization framework. Chatzigeorgiou et al. (2016) have established the representation at different scales of the variables and the conservation/constitutive laws for periodic composites under strong thermomechanical couplings. The same scale separation rules are assumed to have more general validity and to hold for any type of multiscale analysis. Thus, they are applied also here.

In a fully coupled thermomechanical framework under small strains and rotations assumption, the essential implicated fields are the following: the displacement vector $\boldsymbol{u}$, the strain tensor $\boldsymbol{\varepsilon}$, the stress tensor $\boldsymbol{\sigma}$, the temperature θ, the temperature gradient vector $\boldsymbol{\nabla\theta}$, the heat flux vector $\boldsymbol{q}$ and the specific entropy per unit volume s. For generalized standard materials, one needs to identify also a set of internal state variables $\boldsymbol{\zeta}$ (Halphen and Nguyen, 1975; Germain et al., 1983). In addition, applying the thermodynamic prin-

ciples requires the introduction of certain energies and energy rates terms: the internal energy per unit volume U, the Helmholtz free energy potential Ψ and the intrinsic dissipation γ_{loc}.

For a homogeneous continuum body, the displacements and strains are related through the kinematics relation

$$\boldsymbol{\varepsilon} = \frac{1}{2}\left[\frac{\partial \boldsymbol{u}}{\partial \boldsymbol{x}} + \left[\frac{\partial \boldsymbol{u}}{\partial \boldsymbol{x}}\right]^T\right], \tag{1}$$

where the superscript ^{T} denotes the transpose of a tensor and $\dfrac{\partial\{\bullet\}}{\partial \boldsymbol{x}}$ represents gradient of a vector. On the other hand, the equilibrium equation, ignoring inertia and body forces, is written as

$$\text{div}\boldsymbol{\sigma} = \boldsymbol{0}, \tag{2}$$

where $\text{div}\,\{\bullet\}$ denotes the divergence of a tensor or vector. In addition, the first law of thermodynamics (i.e. energy balance equation) without the presence of heat sources reads

$$Q + r = 0, \quad Q = -\text{div}\boldsymbol{q}, \quad r = \boldsymbol{\sigma} : \dot{\boldsymbol{\varepsilon}} - \dot{U}. \tag{3}$$

In the above expressions, the dot above a symbol represents time derivative, while : stands for the double contraction operator between tensors. The second law of thermodynamics in the strong form of Clausius-Duhem inequality is written as

$$\gamma = \theta\dot{s} + \boldsymbol{\sigma} : \dot{\boldsymbol{\varepsilon}} - \dot{U} - \frac{1}{\theta}\boldsymbol{q} \cdot \boldsymbol{\nabla}\boldsymbol{\theta} \geqslant 0. \tag{4}$$

It is noted that $\cdot$ stands for the single contraction operator between vectors or tensors. The latter inequality is utilized to establish thermodynamically

consistent constitutive laws for the materials. To achieve that, the internal energy is substituted by another potential, like the Helmholtz free energy, which depends on the strain tensor, the temperature and the set of internal variables. The transformation between U and Ψ is written as

$$\Psi = U - s\theta. \tag{5}$$

Combining (4) and (5) and considering the standard thermodynamics arguments (Coleman and Gurtin, 1967; Lubliner, 1972; Germain et al., 1983), the following relations hold:

$$\boldsymbol{\sigma} = \frac{\partial \Psi}{\partial \boldsymbol{\varepsilon}}, \qquad s = -\frac{\partial \Psi}{\partial \theta}. \tag{6}$$

Moreover, the total dissipation γ is split in two parts: the local entropy production, or intrinsic dissipation,

$$\gamma_{\text{loc}} = \theta \dot{s} + r = -\frac{\partial \Psi}{\partial \boldsymbol{\zeta}} * \dot{\boldsymbol{\zeta}}, \tag{7}$$

and the entropy production by heat conduction

$$\gamma_{\text{con}} = -\frac{1}{\theta} \boldsymbol{q} \cdot \boldsymbol{\nabla \theta}. \tag{8}$$

Both terms should be independently non-negative for a generalized standard material. It should be mentioned that the operator $*$ denotes product according to the nature of $\boldsymbol{\zeta}$; for scalar it is the usual product, for vector it is single contraction, and for second order tensor it is double contraction.

The above thermodynamic framework is well established for homogeneous media. When dealing with composites, multiscale procedures require to establish relations between the fields at the different scales, as well as to define

the important relations (conservation laws, constitutive equations, kinematics etc) at every implicated scale. For a two-scale medium, the asymptotic expansion approach at the zeroth order homogenization theory reveals that the displacement vector and the temperature are strongly convergent fields (Ene, 1983; Yu and Fish, 2002; Chatzigeorgiou et al., 2016, 2018; Tikarrouchine et al., 2019); when the size of the microscale level is very small compared to the size of the actual structure, the microfluctuations of $\boldsymbol{u}$ and θ tend to vanish, i.e. the microscopic and macroscopic quantities coincide. However, their gradients (strain for the displacement and temperature gradient for the temperature) are highly oscillating fields at the microscale, thus one has to identify their average as macroscopic counterparts.

In the sequel, the microscopic fields and quantities appear with regular notation, while their macroscopic counterparts appear with a bar above the symbol. Also, the symbol $\langle\{\bullet\}\rangle$ denotes the volume average of a quantity at the RVE.

Table 1 provides the list of important fields and their representation at both microscale and macroscale. It should be noted that, since the temperature is a strongly convergent field, the microscopic Helmholtz free energy depends on the macroscopic temperature $\bar{\theta}$. Also, while the intrinsic dissipation at the microscale can be written in an explicit form as the product of two terms, such representation cannot be given in a strict sense for its macroscopic counterpart. However, $\bar{\gamma}_{\text{loc}}$ can be identified as the volume average of the microscopic γ_{loc} in the RVE.

Table 2 contains the main equations at the two scales. In the latter Table, the terms $\boldsymbol{u}$ and θ are microscale fluctuating terms of the displacement vector

variable	microscale	macroscale
Helmholtz free energy potential	$\Psi\left(\boldsymbol{\varepsilon}, \bar{\theta}, \boldsymbol{\zeta}\right)$	$\overline{\Psi} = \langle \Psi \rangle$
intrinsic dissipation	$\gamma_{\text{loc}} = -\dfrac{\partial \Psi}{\partial \boldsymbol{\zeta}} * \dot{\boldsymbol{\zeta}}$	$\bar{\gamma}_{\text{loc}} = \langle \gamma_{\text{loc}} \rangle$
strain	$\boldsymbol{\varepsilon}$	$\bar{\boldsymbol{\varepsilon}} = \langle \boldsymbol{\varepsilon} \rangle$
stress	$\boldsymbol{\sigma} = \dfrac{\partial \Psi}{\partial \boldsymbol{\varepsilon}}$	$\overline{\boldsymbol{\sigma}} = \langle \boldsymbol{\sigma} \rangle$
temperature gradient	$\boldsymbol{\nabla \theta}$	$\overline{\boldsymbol{\nabla \theta}} = \langle \boldsymbol{\nabla \theta} \rangle$
heat flux	$\boldsymbol{q}$	$\bar{\boldsymbol{q}} = \langle \boldsymbol{q} \rangle$
specific entropy per unit volume	$s = -\dfrac{\partial \Psi}{\partial \bar{\theta}}$	$\bar{s} = \langle s \rangle$
internal energy per unit volume	U	$\overline{U} = \langle U \rangle$

Table 1: Thermomechanical fields at microscale and macroscale.

and the temperature. As the size of the RVE tends to zero (compared to the actual macrostructure), these fluctuations are very small. However, their gradients $\dfrac{\partial \boldsymbol{u}}{\partial \boldsymbol{x}}$ and $\dfrac{\partial \theta}{\partial \boldsymbol{x}}$ are highly oscillating, and thus they still appear on the strain tensor and the temperature gradient respectively. Moreover,

$$\left\langle \frac{\partial \boldsymbol{u}}{\partial \boldsymbol{x}} \right\rangle = \mathbf{0}, \qquad \left\langle \frac{\partial \theta}{\partial \boldsymbol{x}} \right\rangle = \mathbf{0}.$$

Tables 1 and 2 summarize the general framework of homogenization for composites under fully coupled thermomechanical conditions (Chatzigeorgiou et al., 2016). The next sections focus on a specific mean-field micromechanics technique, namely the Mori-Tanaka theory (Mori and Tanaka, 1973;

equation	microscale	macroscale
kinematics	$\boldsymbol{\varepsilon} = \bar{\boldsymbol{\varepsilon}} + \frac{1}{2}\left[\frac{\partial \boldsymbol{u}}{\partial \boldsymbol{x}} + \left[\frac{\partial \boldsymbol{u}}{\partial \boldsymbol{x}}\right]^T\right]$	$\overline{\boldsymbol{\varepsilon}} = \frac{1}{2}\left[\frac{\partial \overline{\boldsymbol{u}}}{\partial \overline{\boldsymbol{x}}} + \left[\frac{\partial \overline{\boldsymbol{u}}}{\partial \overline{\boldsymbol{x}}}\right]^T\right]$
equilibrium	$\mathrm{div}\boldsymbol{\sigma} = \boldsymbol{0}$	$\overline{\mathrm{div}}\overline{\boldsymbol{\sigma}} = \boldsymbol{0}$
temperature gradient	$\boldsymbol{\nabla\theta} = \overline{\boldsymbol{\nabla}}\bar{\boldsymbol{\theta}} + \frac{\partial \theta}{\partial \boldsymbol{x}}$	$\overline{\boldsymbol{\nabla}}\bar{\boldsymbol{\theta}} = \frac{\partial \bar{\theta}}{\partial \overline{\boldsymbol{x}}}$
energy equation	$\mathrm{div}\boldsymbol{q} = 0$	$\overline{\mathrm{div}}\overline{\boldsymbol{q}} = \overline{\boldsymbol{\sigma}} : \dot{\bar{\boldsymbol{\varepsilon}}} - \dot{\bar{U}}$
dissipation inequality	$\bar{\theta}\dot{s} + \boldsymbol{\sigma} : \dot{\boldsymbol{\varepsilon}}$ $-\dot{U} - \frac{1}{\bar{\theta}}\boldsymbol{q} \cdot \boldsymbol{\nabla\theta} \geqslant 0$	$\bar{\theta}\dot{\bar{s}} + \overline{\boldsymbol{\sigma}} : \dot{\bar{\boldsymbol{\varepsilon}}}$ $-\dot{\bar{U}} - \frac{1}{\bar{\theta}}\overline{\boldsymbol{q}} \cdot \overline{\boldsymbol{\nabla}}\bar{\boldsymbol{\theta}} \geqslant 0$
Helmholtz-internal energy relation	$\Psi = U - s\bar{\theta}$	$\overline{\Psi} = \bar{U} - \bar{s}\bar{\theta}$
rate of Helmholtz free energy	$\dot{\Psi} = \boldsymbol{\sigma} : \dot{\boldsymbol{\varepsilon}} - s\dot{\bar{\theta}} + \frac{\partial \Psi}{\partial \boldsymbol{\zeta}} * \dot{\boldsymbol{\zeta}}$	$\dot{\overline{\Psi}} = \overline{\boldsymbol{\sigma}} : \dot{\bar{\boldsymbol{\varepsilon}}} - \bar{s}\dot{\bar{\theta}} - \bar{\gamma}_{\mathrm{loc}}$

Table 2: Basic equations at microscale and macroscale

Benveniste, 1987) combined with the Transformation Field Analysis (Dvorak, 1992; Dvorak and Benveniste, 1992).

3. Formulation of Mori-Tanaka/TFA homogenization for fully coupled thermomechanical processes

Considering a fully coupled thermomechanical process, the objective of this section is to provide a homogenization framework that computes the mechanical and thermal fields as well as the thermomechanical tangent moduli.

In mean-field homogenization theories, the fields are estimated in an average sense per material phase. Let us assume an $N+1$ multiphase medium, in which the matrix is noted with the index 0, while the various reinforcements are noted with indices between the values of 1 to N.

The Mori-Tanaka methodology is a well-known mean-field approach that utilizes the Eshelby solution. From the Eshelby inhomogeneity problem one can establish the so-called dilute concentration tensors for the reinforcement, which in a second step are used to compute the total concentration tensors (Chatzigeorgiou et al., 2018, 2022). When dealing with coupled thermomechanical problems, it is important to establish mechanical and thermal type of concentration tensors.

Before passing to the actual micromechanics scheme, it is useful to introduce the consitutive law in a generic manner that allows to apply a homogenization framework.

3.1. Phases constitutive laws

For a phase i ($i = 0, 1, ..., N$), the stress-strain relation $(6)_1$ for a medium experiencing thermal and inelastic strains, as well as damage mechanisms,

can be written in the general form

$$\boldsymbol{\sigma}_i = \boldsymbol{D}_i : [\boldsymbol{\varepsilon}_i - \boldsymbol{\varepsilon}_i^p - \boldsymbol{a}_i[\bar{\theta} - \bar{\theta}_{\text{ref}}]] = \boldsymbol{D}_i : \boldsymbol{\varepsilon}_i + \boldsymbol{\sigma}_i^p, \tag{9}$$

where $\boldsymbol{D}_i$ is the secant modulus tensor (i.e. reduced elasticity modulus due to damage effects), $\boldsymbol{a}_i$ is the thermal expansion tensor, $\bar{\theta}_{\text{ref}}$ is the reference temperature, $\boldsymbol{\varepsilon}_i^p$ is the total inelastic strain due to nonlinear mechanisms (plasticity, viscoelasticity, viscoplasticity etc.) and $\boldsymbol{\sigma}_i^p$ is the sum of inelastic and thermal stresses.

The notion of secant modulus is frequently utilized in the literature and is different from the concept of the tangent modulus (described later in the manuscript). For an isotropic medium whose damage state is represented through a single scalar damage parameter d, the relation between the secant modulus $\boldsymbol{D}_i$ and the elasticity modulus $\boldsymbol{C}_i$ is given by

$$\boldsymbol{D}_i = [1 - d]\boldsymbol{C}_i.$$

Concerning the thermal fields, the heat flux-temperature gradient consitutive law for the same phase i is expressed through the Fourier's law

$$\boldsymbol{q}_i = -\boldsymbol{\kappa}_i \cdot \boldsymbol{\nabla}\boldsymbol{\theta}_i, \tag{10}$$

where $\boldsymbol{\kappa}_i$ denotes the thermal conductivity second order tensor. Finally, the energy rate term r of the phase i for the first law of thermodynamics is written with the help of equation (7) as

$$r_i = -\bar{\theta}\dot{s}_i + \gamma_{\text{loc}_i}, \tag{11}$$

where s_i is the entropy per unit volume and γ_{loc_i} is the intrinsic dissipation of that phase.

3.2. Dilute concentration tensors

When dealing with mean-field homogenization methods, the Eshelby inhomogeneity problems lead to the estimation of the so-called dilute concentration tensors. The mechanical and thermal inhomogeneity problems are described schematically in Figure 1. In both cases, a single inhomogeneity of ellipsoidal shape is embedded in an infinite body.

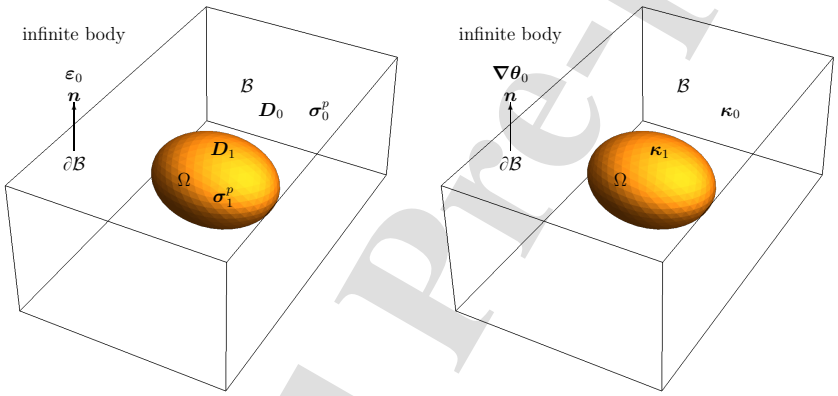

(a) Mechanical problem (b) Thermal problem

Figure 1: Eshelby inhomogeneity problems for mechanical and thermal fields.

Mechanical part: With respect to the mechanical fields, the infinite body is characterized by the secant modulus tensor $\boldsymbol{D}_0$ and is subjected to inelastic stress $\boldsymbol{\sigma}_0^p$. The inhomogeneity has secant modulus $\boldsymbol{D}_1$ and is subjected to inelastic stress $\boldsymbol{\sigma}_1^p$. At far distance, the medium is subjected to uniform strain $\boldsymbol{\varepsilon}_0$ (Figure 1_a). The inhomogeneity has ellipsoidal shape. The solution of the Eshelby problem for this case leads to the conclusion that the strain in the inhomogeneity is given by the following expression (Chatzigeorgiou and

Meraghni, 2019; Chatzigeorgiou et al., 2022)

$$\boldsymbol{\varepsilon}_1 = \boldsymbol{T}_1 : \boldsymbol{\varepsilon}_0 + \boldsymbol{T}_1^p : \boldsymbol{\sigma}_0^p - \boldsymbol{T}_1^p : \boldsymbol{\sigma}_1^p, \tag{12}$$

with

$$\begin{aligned} \boldsymbol{T}_1 &= \left[\boldsymbol{\mathcal{I}} + \boldsymbol{P}_1 : [\boldsymbol{D}_1 - \boldsymbol{D}_0]\right]^{-1}, \\ \boldsymbol{T}_1^p &= \boldsymbol{T}_1 : \boldsymbol{P}_1, \\ \boldsymbol{P}_1 &= \boldsymbol{S}(\boldsymbol{D}_0) : \boldsymbol{D}_0^{-1}. \end{aligned} \tag{13}$$

The $\boldsymbol{S}$ denotes the Eshelby tensor. It is worth mentioning that in equation (12), $\boldsymbol{T}_1$ represents the classical dilute concentration tensor of the Eshelby-based approaches, while the tensor $\boldsymbol{T}_1^p$ serves for the introduction of the TFA method in the final composite.

Thermal part: Analogy exists between the thermal and the mechanical Eshelby problem. With respect to the thermal fields, the infinite body is characterized by the thermal conductivity tensor $\boldsymbol{\kappa}_0$. The inhomogeneity has thermal conductivity tensor $\boldsymbol{\kappa}_1$ and at far distance, the medium is subjected to uniform temperature gradient $\boldsymbol{\nabla\theta}_0$ (Figure 1_b). The Eshelby problem for the thermal conductivity leads to the expression (Chatzigeorgiou et al., 2018)

$$\boldsymbol{\nabla\theta}_1 = \boldsymbol{T}_1^{\kappa} \cdot \boldsymbol{\nabla\theta}_0, \tag{14}$$

with

$$\begin{aligned} \boldsymbol{T}_1^{\kappa} &= \left[\boldsymbol{I} + \boldsymbol{P}_1^{\kappa} : [\boldsymbol{\kappa}_1 - \boldsymbol{\kappa}_0]\right]^{-1}, \\ \boldsymbol{P}_1^{\kappa} &= \boldsymbol{S}^{\kappa}(\boldsymbol{\kappa}_0) : \boldsymbol{\kappa}_0^{-1}. \end{aligned} \tag{15}$$

The $\boldsymbol{S}^{\kappa}$ denotes the thermal Eshelby tensor (Hatta and Taya, 1986).

3.3. Mori-Tanaka concentration tensors for N+1 phases

After solving the Eshelby inhomogeneity problem, one can pass to the composite material. Let's assume a composite whose RVE consists of a matrix phase and multiple inhomogeneities of ellipsoidal shape.

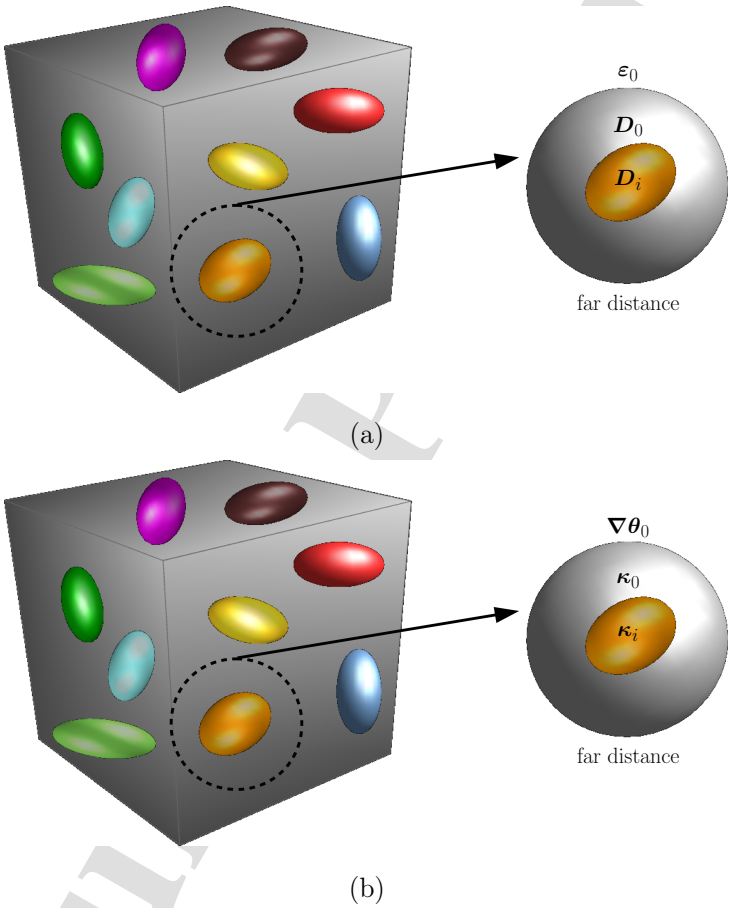

Figure 2: Mori-Tanaka hypothesis for each inhomogeneity at an RVE: (a) Mechanical problem. (b) Thermal problem.

Mechanical part: Figure 2_a demonstrates the major hypothesis of the

Mori-Tanaka scheme for the mechanical problem: In an RVE, each inhomogeneity with its surrounding matrix is treated as an Eshelby problem. At the far field of this hypothetical problem the boundary conditions provide a strain field equal to the average strain in the matrix.

The results of the previous subsection need to be extended in order to account for N inhomogeneities in a matrix. Equation (12) can be written in a more general manner for the i_{th} inhomogeneity as

$$\boldsymbol{\varepsilon}_i = \boldsymbol{T}_i : \boldsymbol{\varepsilon}_0 + \boldsymbol{T}_i^p : \boldsymbol{\sigma}_0^p - \boldsymbol{T}_i^p : \boldsymbol{\sigma}_i^p. \tag{16}$$

From the definition of the macroscopic strain in a composite with N inhomogeneities, one has

$$\bar{\boldsymbol{\varepsilon}} = c_0 \boldsymbol{\varepsilon}_0 + \sum_{i=1}^{N} c_i \boldsymbol{\varepsilon}_i, \tag{17}$$

where c_i stands for the volume fraction of the i_{th} inhomogeneity and c_0 is the volume fraction of the matrix. Integrating (16) into (17) yields

$$\boldsymbol{\varepsilon}_0 = \boldsymbol{A}_0 : \bar{\boldsymbol{\varepsilon}} + \boldsymbol{A}_0^p : \boldsymbol{\sigma}_0^p + \sum_{i=1}^{N} \boldsymbol{A}_{i,0}^p : \boldsymbol{\sigma}_i^p, \tag{18}$$

with

$$\begin{aligned} \boldsymbol{A}_0 &= \left[c_0 \boldsymbol{\mathcal{I}} + \sum_{i=1}^{N} c_i \boldsymbol{T}_i \right]^{-1}, \\ \boldsymbol{A}_{i,0}^p &= c_i \boldsymbol{A}_0 : \boldsymbol{T}_i^p, \\ \boldsymbol{A}_0^p &= -\boldsymbol{A}_0 : \left[\sum_{i=1}^{N} c_i \boldsymbol{T}_i^p \right] = -\sum_{i=1}^{N} \boldsymbol{A}_{i,0}^p. \end{aligned} \tag{19}$$

Implementing these results to (16) yields (Chatzigeorgiou and Meraghni, 2019)

$$\boldsymbol{\varepsilon}_i = \boldsymbol{A}_i : \bar{\boldsymbol{\varepsilon}} + \boldsymbol{A}_{0,i}^p : \boldsymbol{\sigma}_0^p + \sum_{j=1}^{N} \boldsymbol{A}_{j,i}^p : \boldsymbol{\sigma}_j^p, \tag{20}$$

where

$$\begin{aligned} \boldsymbol{A}_i &= \boldsymbol{T}_i : \boldsymbol{A}_0, \\ \boldsymbol{A}^p_{0,i} &= \boldsymbol{T}_i : \boldsymbol{A}^p_0 + \boldsymbol{T}^p_i, \\ \boldsymbol{A}^p_{j,i} &= \begin{cases} \boldsymbol{T}_i : \boldsymbol{A}^p_{i,0} - \boldsymbol{T}^p_i & j = i, \\ \boldsymbol{T}_i : \boldsymbol{A}^p_{j,0} & j \neq i. \end{cases} \end{aligned} \tag{21}$$

In the expressions (18), (20), the first terms represent the usual Mori-Tanaka scheme, while the additional terms related to the inelastic stresses integrate the TFA theory. According to this method, the total strain at each phase depends on the the macroscopic strain and the inelastic stresses of all material phases. The contribution of each $\boldsymbol{\sigma}^p_j$ on the i_{th} phase total strain is determined through the inelastic concentration tensor $\boldsymbol{A}^p_{j,i}$.

As a side note, the macroscopic secant modulus is given by the relation

$$\overline{\boldsymbol{D}} = c_0 \boldsymbol{D}_0 : \boldsymbol{A}_0 + \sum_{i=1}^{N} c_i \boldsymbol{D}_i : \boldsymbol{A}_i. \tag{22}$$

Thermal part: In analogy to the mechanical problem, the Mori-Tanaka for the thermal fields is based on a similar hypothesis (Figure 2_b): In an RVE, each inhomogeneity with its surrounding matrix is treated as an Eshelby problem. At the far field of this hypothetical problem the boundary conditions provide a temperature gradient field equal to the average temperature gradient in the matrix. Equation (14) can be written in a more general manner for the i_{th} inhomogeneity as

$$\boldsymbol{\nabla\theta}_i = \boldsymbol{T}^{\kappa}_i \cdot \boldsymbol{\nabla\theta}_0. \tag{23}$$

From the definition of the macroscopic temperature gradient in a composite

with N inhomogeneities, one has

$$\overline{\boldsymbol{\nabla\theta}} \;=\; c_0\boldsymbol{\nabla\theta}_0 + \sum_{i=1}^{N} c_i\boldsymbol{\nabla\theta}_i.$$

The last expression leads to

$$\boldsymbol{\nabla\theta}_0 = \boldsymbol{A}_0^{\kappa}\cdot\overline{\boldsymbol{\nabla\theta}}, \tag{24}$$

with

$$\boldsymbol{A}_0^{\kappa} = \left[c_0\boldsymbol{I} + \sum_{i=1}^{N} c_i\boldsymbol{T}_i^{\kappa}\right]^{-1}. \tag{25}$$

Implementing these results to (23) yields

$$\boldsymbol{\nabla\theta}_i = \boldsymbol{A}_i^{\kappa}\cdot\overline{\boldsymbol{\nabla\theta}}, \tag{26}$$

where

$$\boldsymbol{A}_i^{\kappa} = \boldsymbol{T}_i^{\kappa} : \boldsymbol{A}_0^{\kappa}. \tag{27}$$

As a side note, the thermal conductivity tensor of the overall composite is computed through the relation

$$\overline{\boldsymbol{\kappa}} = \sum_{i=0}^{N} c_i\boldsymbol{\kappa}_i\cdot\boldsymbol{A}_i^{\kappa}. \tag{28}$$

3.4. Macroscopic tangent moduli computation

For thermomechanical analyses the computations of tangent moduli are important when dealing with the finite element method. The procedure discussed here follows the methodology introduced in Chatzigeorgiou et al. (2018).

The four thermomechanical tangent moduli

$$\overline{\boldsymbol{D}}^{\varepsilon} = \frac{\partial \overline{\boldsymbol{\sigma}}}{\partial \overline{\boldsymbol{\varepsilon}}}, \quad \overline{\boldsymbol{D}}^{\theta} = \frac{\partial \overline{\boldsymbol{\sigma}}}{\partial \overline{\theta}}, \quad \overline{\boldsymbol{R}}^{\varepsilon} = \frac{\partial \overline{r}}{\partial \overline{\boldsymbol{\varepsilon}}}, \quad \overline{R}^{\theta} = \frac{\partial \overline{r}}{\partial \overline{\theta}},$$

of the composite are computed from the constituents' counterparts

$$\boldsymbol{D}_i^{\varepsilon} = \frac{\partial \boldsymbol{\sigma}}{\partial \boldsymbol{\varepsilon}}, \quad \boldsymbol{D}_i^{\theta} = \frac{\partial \boldsymbol{\sigma}}{\partial \overline{\theta}}, \quad \boldsymbol{R}_i^{\varepsilon} = \frac{\partial r}{\partial \boldsymbol{\varepsilon}}, \quad R_i^{\theta} = \frac{\partial r}{\partial \overline{\theta}},$$

through the relations

$$\begin{aligned} \overline{\boldsymbol{D}}^{\varepsilon} &= \sum_{i=0}^{N} c_i \boldsymbol{D}_i^{\varepsilon} : \boldsymbol{A}_i^{\varepsilon}, \quad \overline{\boldsymbol{D}}^{\theta} = \sum_{i=0}^{N} c_i \left[\boldsymbol{D}_i^{\theta} + \boldsymbol{D}_i^{\varepsilon} : \boldsymbol{A}_i^{\theta} \right], \\ \overline{\boldsymbol{R}}^{\varepsilon} &= \sum_{i=0}^{N} c_i \boldsymbol{R}_i^{\varepsilon} : \boldsymbol{A}_i^{\varepsilon}, \quad \overline{R}^{\theta} = \sum_{i=0}^{N} c_i \left[R_i^{\theta} + \boldsymbol{R}_i^{\varepsilon} : \boldsymbol{A}_i^{\theta} \right], \end{aligned} \tag{29}$$

where the concentration tensors are computed from the Mori-Tanaka scheme according to the formulas

$$\begin{aligned} \boldsymbol{A}_i^{\varepsilon} = \boldsymbol{T}_i^{\varepsilon} : \boldsymbol{A}_0^{\varepsilon}, \quad \boldsymbol{A}_0^{\varepsilon} = \left[c_0 \boldsymbol{\mathcal{I}} + \sum_{j=1}^{N} c_j \boldsymbol{T}_j^{\varepsilon} \right]^{-1}, \\ \boldsymbol{A}_i^{\theta} = \boldsymbol{T}_i^{\varepsilon} : \boldsymbol{A}_0^{\theta} + \boldsymbol{T}_i^{\theta}, \quad \boldsymbol{A}_0^{\theta} = -\boldsymbol{A}_0^{\varepsilon} : \left[\sum_{j=1}^{N} c_j \boldsymbol{T}_j^{\theta} \right], \end{aligned} \tag{30}$$

with

$$\begin{aligned} \boldsymbol{T}_i^{\varepsilon} &= \left[\boldsymbol{\mathcal{I}} + \boldsymbol{P}_i : [\boldsymbol{D}_i^{\varepsilon} - \boldsymbol{D}_0^{\varepsilon}] \right]^{-1}, \\ \boldsymbol{T}_r^{\theta} &= [\boldsymbol{\mathcal{I}} - \boldsymbol{T}_r^{\varepsilon}] : [\boldsymbol{D}_0^{\varepsilon} - \boldsymbol{D}_i^{\varepsilon}]^{-1} : [\boldsymbol{D}_i^{\theta} - \boldsymbol{D}_0^{\theta}]. \end{aligned} \tag{31}$$

The polarization (or Hill) tensors $\boldsymbol{P}_i$ are computed using the mechanical tangent modulus $\boldsymbol{D}_0^{\varepsilon}$ and the relevant Eshelby tensors.

3.5. Numerical implementation

For the micromechanics scheme described previously, a numerical algorithm is designed that can be adopted for structural applications. The algorithm follows the standard structure of a typical thermomechanical User Material (UMAT) subroutine for the ABAQUS FE software. In a UMAT, the inputs are all the variables at the previous time step n. For the total strain and the temperature, their time increments are provided at the current time step $n+1$ (thus, these fields are also known at the current time step). The outputs contain the updated stresses, the internal variables and the energy rate term r at the time step $n+1$, as well as the four thermomechanical tangent moduli. It is noted that for the thermal part of the problem, the macroscopic thermal conductivity is computed only once at the beginning of the analysis. This approach is valid here, since the thermal conductivities of all material constituents are considered constants. It should be pointed out that, even if the constituents' thermal conductivities depend on the temperature, the calculations are not altered significantly. According to the zeroth order homogenization approach, $\bar{\theta}$ is uniform throughout the RVE. Thus, the macroscopic thermal conductivity can be estimated once as a function of the macroscopic temperature prior to the main thermomechanical analysis.

For every material phase, a proper subroutine is designed according to the phase's constitutive law. Such subroutines follow the standard return mapping algorithm methodology (Simo and Hughes, 1998; Chatzigeorgiou et al., 2018). For the overall composite, the Mori-Tanaka/TFA approach is performed through a Meta-UMAT subroutine, whose structure is presented in Figure 3.

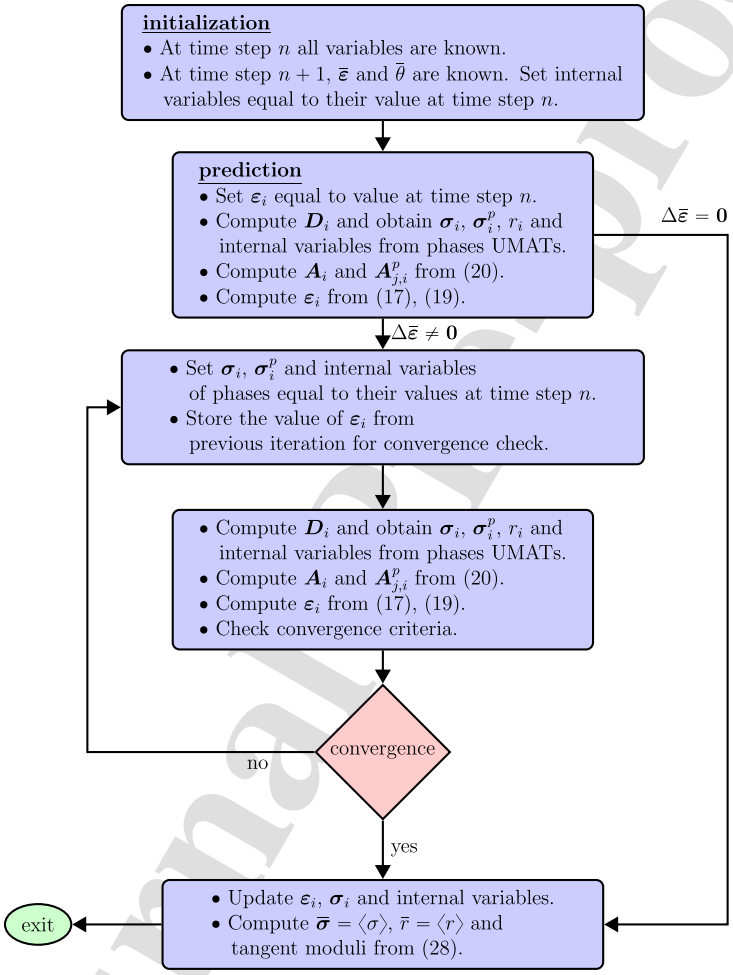

Figure 3: Computational algorithm (Meta-UMAT) for the thermomechanical homogenization of multilayered composites. Mori-Tanaka/TFA approach. The symbol Δ denotes time increment.

4. Numerical examples

In this section, various numerical examples demonstrate the accuracy and capabilities of the proposed framework.

4.1. Multilayered structure: comparison with periodic homogenization

The first example deals with a multilayered structure which was studied in Chatzigeorgiou et al. (2016) using the periodic homogenization method and founded on asymptotic expansion.

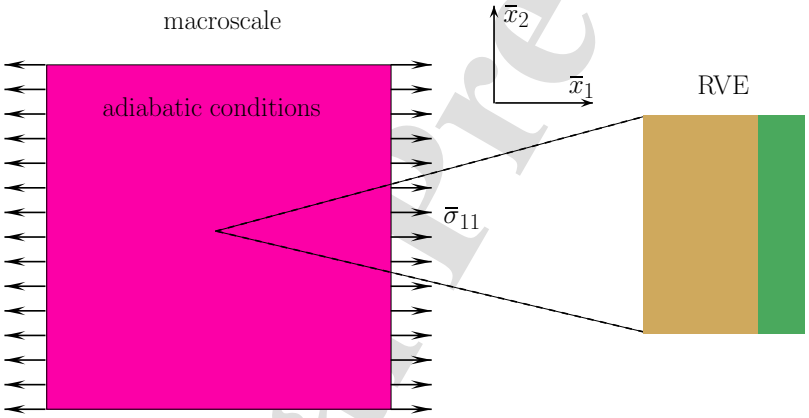

Figure 4: Multilayered structure under uniaxial loading and adiabatic conditions. The RVE consists of two layers, an epoxy (20% volume fraction) and a steel 316 (80% volume fraction).

A multilayered composite plate is subjected to stress controlled uniaxial loading at the direction 1, while it is under adiabatic conditions (Figure 4). The stress boundary conditions are applied in three steps:

1. loading up to 200 MPa and subsequent unloading,
2. loading up to 220 MPa and subsequent unloading,

3. loading up to 240 MPa and subsequent unloading.

The stress rate is always 1 MPa/s.

property	steel 316	epoxy
Young modulus [MPa]	185000	3000
Poisson ratio	0.27	0.3
thermal expansion [1/K]	1.5E-5	1.1E-4
density [t/m^3]	7.8	1.12
specific heat capacity [MPa m^3/(t K)]	0.5	1.64
thermal conductivity [MPa m^2/(s K)]	1.5E-5	0.4E-6
elastic limit Y [MPa]	84	
K_a [MPa/s$^{1/N_a}$]	151	
N_a	24	
Q_1 [MPa]	6400	
Q_2 [MPa]	270	
b	25	

Table 3: Thermomechanical properties of constituents for the structure of Figure 4. The steel 316 mechanical properties have been obtained from Lemaitre and Chaboche (2002).

The RVE of the composite consists of two layers, an epoxy (20% volume fraction) and steel 316 (80% volume fraction). The former has thermoelastic behavior, while the latter has J_2 thermoviscoplastic behavior. When plastically deformed, the von Mises stress σ^{vM} of the steel 316 material is expressed in terms of the accumulated plastic strain p and its rate according to the relation (Lemaitre and Chaboche, 2002)

$$\sigma^{\mathrm{vM}} = Y + Q_1 p + Q_2[1 - \exp(-bp)] + K_a \dot{p}^{1/N_a}, \tag{32}$$

where Y is the elastic limit, Q_1, Q_2, b are plastic hardening parameters and K_a, N_a are viscous parameters. The entropy in both materials is given by

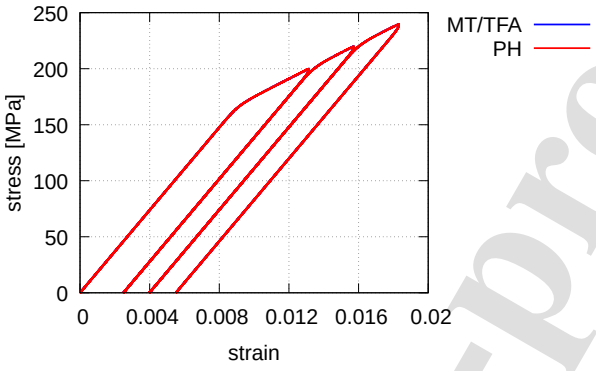

(a)

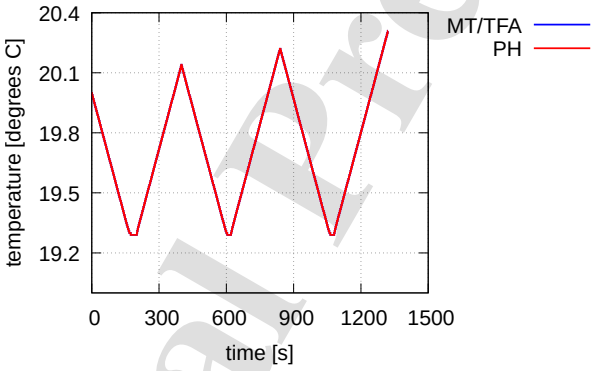

(b)

Figure 5: Multilayered composite with 20% elastic epoxy and 80% viscoplastic steel Chatzigeorgiou et al., 2016: Results comparison between the proposed Mori-Tanaka/TFA (MT/TFA) scheme and the periodic homogenization (PH).

the expression

$$s = \boldsymbol{\alpha} : \boldsymbol{\sigma} + \rho c \ln\left(\frac{\bar{\theta}}{\bar{\theta}_{\text{ref}}}\right), \tag{33}$$

where ρ and c denote the density and the specific heat capacity respectively. The material parameters of the two constituents are given in Table 3. The

initial temperature is equal to 293.15 K.

As illustrated in the results of Figure 5, the Mori-Tanaka/TFA methodology yields the same results with those obtained by the rigorous periodic homogenization (Chatzigeorgiou et al., 2016) for the multilayered structure. The result confirms the findings in Chatzigeorgiou (2022) on multilayered structures and extends them in the case of thermomechanical coupled conditions. The excellent accuracy of the proposed method appears on the mechanical fields (stress-strain curve of Figure 5_a), as well as on the thermal fields (temperature-time curve of Figure 5_b).

4.2. Multilayered structure: comparison with full structural analysis

property	glass	epoxy
Young modulus E [MPa]	72000	3000
Poisson ratio ν	0.22	0.3
thermal expansion α [1/K]	0.6E-5	1.1E-4
density ρ [t/m^3]	2.5	1.12
specific heat capacity c [MPa m^3/(t K)]	0.8	1.64
thermal conductivity κ [MPa m^2/(s K)]	1.0E-6	0.4E-6
elastic limit Y [MPa]		48
K_a [MPa/s$^{1/N_a}$]		30.17
N_a		5
Q_1 [MPa]		100
Q_2 [MPa]		10
b		5

Table 4: Thermomechanical properties of constituents for the structure of Figure 6.

To further demonstrate the accuracy of the proposed micromechanics scheme, simulations on a multilayered structure are performed using the

Mori-Tanaka/TFA method and a full structural analysis.

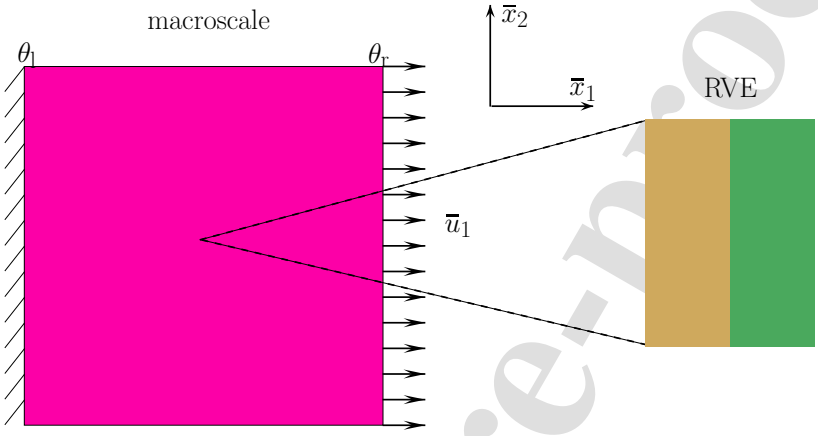

Figure 6: Multilayered structure under uniaxial displacement loading and temperature increase at one external surface. The RVE consists of two layers, an epoxy (50% volume fraction) and a glass (50% volume fraction).

Let's assume a multilayered plate of dimensions 100mm×100mm×8mm, whose RVE consists of two layers of equal volume fraction (50% each). The first layer is an epoxy with thermoviscoplastic response, while the second layer is made of glass with thermoelastic response. The material parameters of the two layers are presented in Table 4. The layers are normal to the axis x_1 and the RVE is repeated 25 times in the total plate. The plate is subjected on one side to a displacement field in the direction 1 and is fixed on the other side. The displacement field increases up to the value of 0.0025 mm with a strain rate of $1.25 \cdot 10^{-4}$ 1/s. The temperature initially is 293.15 K in all the plate. During the duration of 200 s, the $\bar{x}_2 - \bar{x}_3$ right surface is heated up to θ_r =298.15 K (Figure 6).

The analysis of this structure is performed through two ways: a) a full-

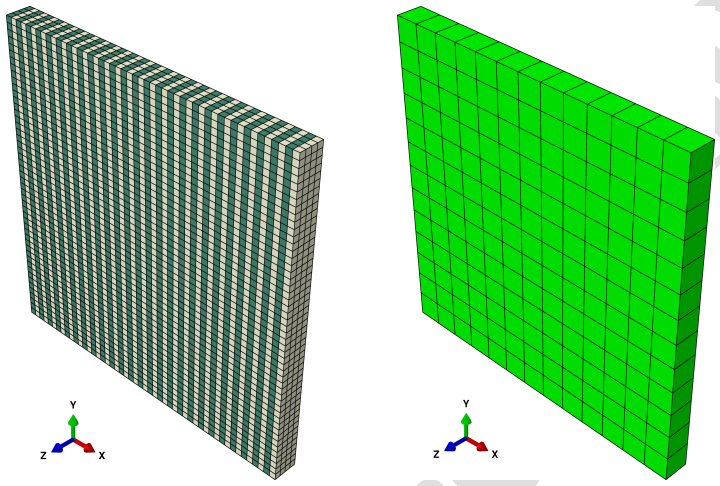

(a) (b)

Figure 7: Multilayered composite with 50% viscoplastic epoxy and 50% elastic glass: Full structure analysis vs Mori-Tanaka/TFA framework. The axes $x-y-z$ in the figure correspond to the global axes $\bar{x}_1-\bar{x}_2-\bar{x}_3$.

structure analysis, where all the microstructural details are included in the FE analysis (Figure 7_a), and b) utilizing the proposed homogenization method for the RVE, while the macro-structure is solved with FE considering a coarse mesh (Figure 7_b).

For the FE computations on the software ABAQUS, using directly the material properties of Table 4 can cause numerical issues. To avoid those, the thermomechanical coupled equations (equilibrium, balance law, constitutive relations) are solved using appropriate normalization. The details of the normalized set of equations for a typical thermoelastic-thermoviscoplastic solid are presented in Appendix A. In the current example, the normalization factors are chosen as: $H = 0.1$ m, $\dot{\gamma}_0 = 1.25 \cdot 10^{-4}$ 1/s, $s_0 = 72000$ MPa, and

$\rho_0 c_0 = 1.9184$ MPa/[t K].

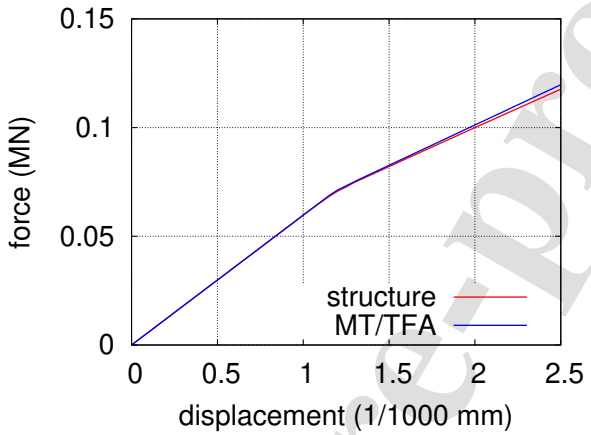

Figure 8: Comparison between full structure analysis and Mori-Tanaka/TFA framework.

Figure 8 demonstrates the force-displacement curve of the studied numerical case using the full-structure analysis and the Mori-Tanaka/TFA homogenization framework. As it can be observed, the developed multiscale approach reproduces very accurately the behavior of the overall plate using much less finite elements for the meshing. Concerning the computational time, in a regular PC (Intel Core i7-8750H CPU at 2.20GHz x 12, 15.3 GB RAM) the Mori-Tanaka/TFA approach requires 35 s compared to 108 s of the full-structure analysis.

4.3. Cylindrical tube made of thermoplastic fiber composite

The last numerical study aims at demonstrating the capabilities of the developed framework. The studied structure is a cylindrical tube made of a PA66 matrix reinforced with unidirectional long glass fibers of 50% volume

property	glass	PA66
Young modulus E [MPa]	72000	3000
Poisson ratio ν	0.22	0.3
thermal expansion α [1/K]	0.6E-5	1.1E-4
density ρ [t/m^3]	2.5	1.12
specific heat capacity c [MPa m^3/(t K)]	0.8	1.64
thermal conductivity κ [MPa m^2/(s K)]	1.0E-6	0.4E-6
elastic limit Y [MPa]		1
K_a [MPa/s$^{1/N_a}$]		45
N_a		2.37
Q_1 [MPa]		260
Q_2 [MPa]		39
b		134
θ_v [K]		29.315

Table 5: Thermomechanical properties of constituents for the fiber composite tube of Figure 9. With the exception of θ_v, the rest of the PA66 properties have been obtained from Nachtane et al. (2022).

fraction. The matrix is a thermoviscoplastic material, while the glass fibers are considered thermoelastic media.

The constitutive law for the PA66 is similar with the one used in the previous examples, with the addition of the temperature influence through a Maxwell probability law for the viscoplastic rate (Lemaitre and Chaboche, 2002):

$$\sigma^{\mathrm{vM}} = Y + Q_1 p + Q_2[1 - \exp(-bp)] + K_a \left[\dot{p} \exp(\theta_v/\theta)\right]^{1/N_a} . \tag{34}$$

Compared to the expression (32), the new material parameter in this viscoplastic law is the θ_v, which represents the activation energy divided by

the universal gas constant. The thermomechanical tangent moduli for this constitutive law are given in the Appendix B. For this numerical study, the material properties for both constituents (matrix and fibers) are summarized in Table 5. The value for θ_v has not been calibrated from experimental data, it has been selected to provide significant interaction between thermal and viscoplastic fields.

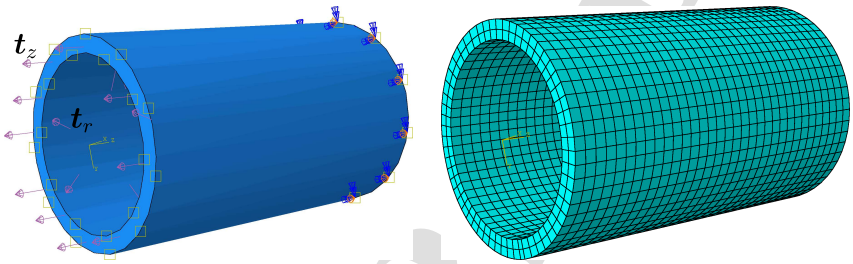

(a) (b)

Figure 9: Cylindrical tube made of fiber composite: (a) Boundary conditions. (b) Meshing.

The tube has a length of 100mm, internal radius 25mm and external radius 30mm. The principal axis of the tube is parallel to the axes of the fibers on the composite material and corresponds to the z direction (Figure 9_a). The numerical calculations have been performed in ABAQUS using 3894 linear hexagonal elements of C3D8T type (Figure 9_b). The loading history has been implemented in 200 time steps. The convergence of the computations has been quite well (3 global iterations at maximum). The computational time of this analysis was 3 hours on the Cassiopee Arts et Métiers Institute of Technology HPC center using 8 mpi processes. This is a significant time improvement compared to FE^2 analysis, which for simpler fiber reinforced structures and single loading cycle requires days of calculations (Tikarrouch-

ine et al., 2019, 2021).

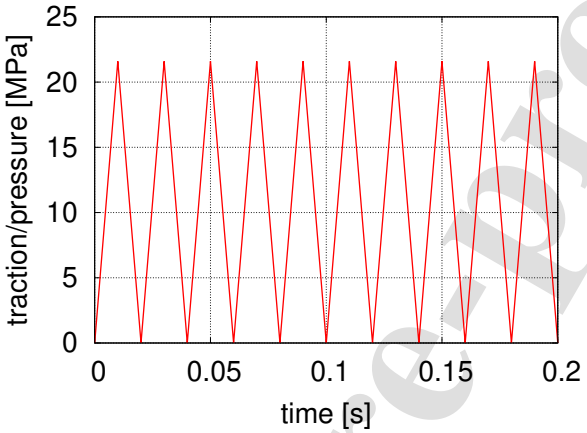

Figure 10: Cyclic loading for traction $\boldsymbol{t}_z$ and pressure $\boldsymbol{t}_r$.

The cylindrical tube is fixed on one end and on the other end is subjected to cyclic traction $\boldsymbol{t}_z$. Also, cyclic internal pressure $\boldsymbol{t}_r = \boldsymbol{t}_z$ is imposed (Figure 9_a). Initially, all the tube is under the same temperature of 293.15 K. The overall time of the analysis is 0.2 s. The cyclic loading for $\boldsymbol{t}_z$ and $\boldsymbol{t}_r$ is illustrated in Figure 10. It represents 10 cycles with frequency of 50 Hz with values between 0 and 21.6 MPa. The tube has zero heat flux at the boundary.

As with the previous numerical example, the computations are performed by normalizing the fields according to the approach discussed in Appendix A. The normalization factors are chosen as: $H = 0.1$ m, $\dot{\gamma}_0 = 1.25 \cdot 10^{-4}$ 1/s, $s_0 = 72000$ MPa, and $\rho_0 c_0 = 1.9184$ MPa/[t K].

The strain profiles at the end of the analysis are illustrated in Figure 11. One can observe the heterogeneity of the components 11 and 22 throughout the tube, while the 33 component is quite uniform at a specific radius.

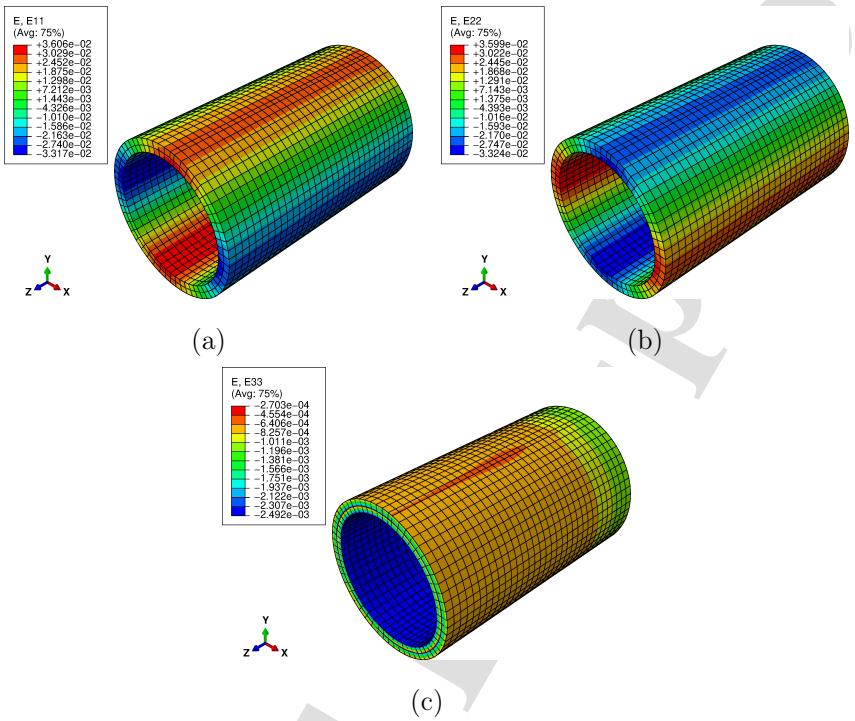

Figure 11: Macroscopic strain profile at time t =0.2 s: (a) component 11, (b) component 22, (c) component 33.

Moreover, the strain levels are below 10%, acceptable for the small strain assumption theory utilized here.

Apart from general profiles, it is interesting to study the evolution of the fields at specific positions of the tube. For illustration reasons, an element, E, and three nodes, A, B and C, are chosen (Figure 12) for demonstrating results in the sequel.

The stress-strain curves at element E for the duration of the ten cycles are given in Figure 13. The three normal components are presented in this

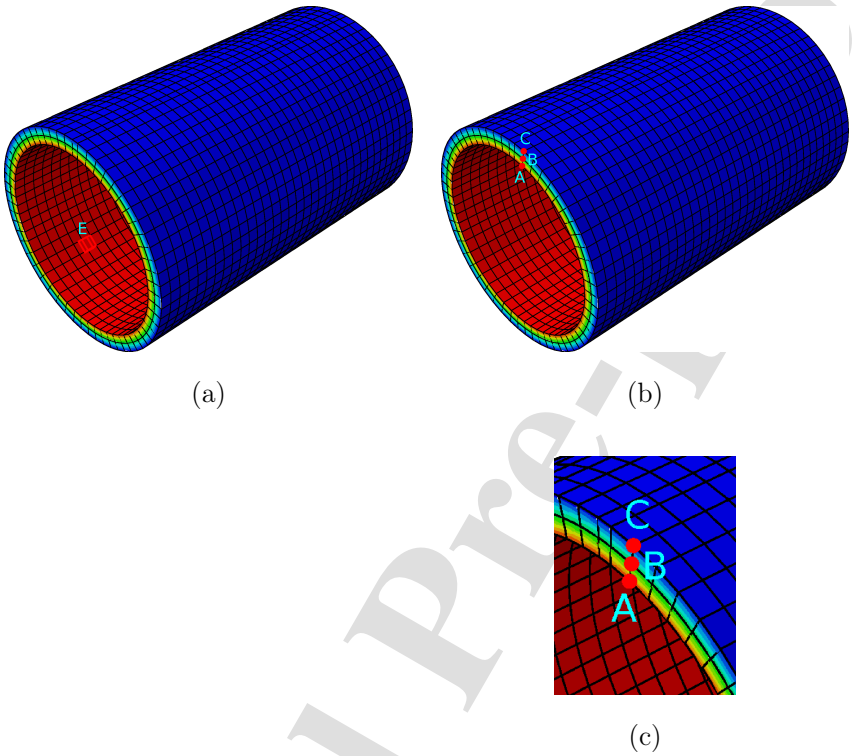

Figure 12: Results on composite tube are presented at: (a) element E, (b) points A, B, C. (c) Zoom of the area with the three points.

Figure. It is observed that the 11 component is the most dominant and accumulates most of the viscoplastic strain. The 33 component, which is parallel to the direction of the tube (and consequently the fibers of the composite) demonstrates very low inelastic effects.

Figure 14_a shows the evolution of the macroscopic intrinsic dissipation $\bar{\gamma}_{\text{loc}}$ at element E with time. As observed, each new cycle generates less dissipation, causing smaller increase in its accumulated value (Figure 14_b). The large development of inelastic mechanisms at the beginning of the cyclic

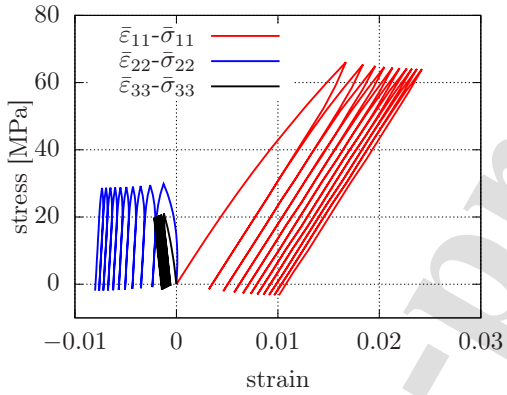

Figure 13: Stress-strain curves at the element E of the tube.

loading is a common phenomenon in polymeric based composites (Chen et al., 2023).

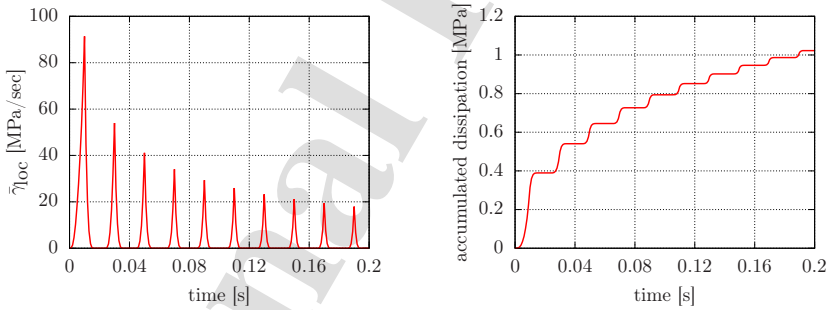

(a) (b)

Figure 14: Macroscopic intrinsic dissipation $\bar{\gamma}_{\mathrm{loc}}$ (a) and its accumulated value (b) versus time at the element E of the tube.

The mean-field homogenization scheme can provide information not only for the macroscopic fields, but also for the average fields per material constituent. Figure 15 illustrates the evolution with time of the viscoplastic

multiplier p for the PA66 matrix corresponding to macroscopic element E. Similarly with the overall dissipation, a large increase of the p occurs at the first cycle, while at consequent cycles its increase is progressive.

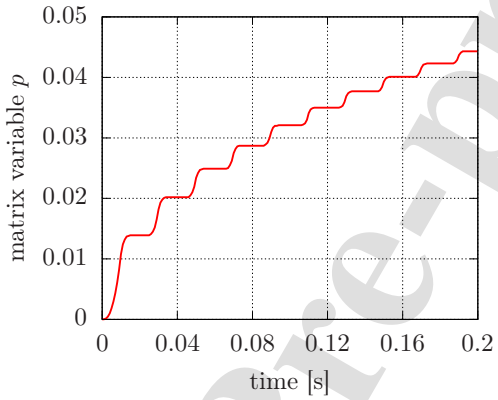

Figure 15: Matrix viscoplastic multiplier p versus time at the element E of the tube.

The evolution of temperature with time at the three selected points, A, B, and C, is demonstrated in Figure 16. The cyclic loading causes cyclic evolution of the temperature. The dissipation leads to an increase of the maximum temperature with each new cycle. At the end of 0.2 s, the temperature has increased by almost 0.7 degrees. It should be noted that the PA66 model considered here does not take into account viscoelasticity and damage. These mechanisms produce significantly more dissipation and higher temperature increase at the end of the loading history.

Closing this example, it is worth pointing out the following: It is well-known that mean-field homogenization techniques for fiber reinforced composites usually lead to stiff mechanical response when nonlinear mechanisms appear on the material constituents (especially the matrix phase). This ef-

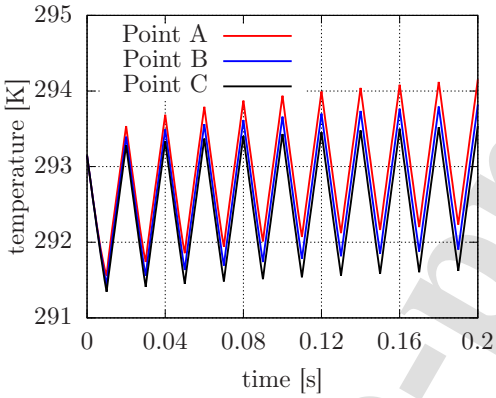

Figure 16: Evolution of temperature with time at the points A, B, C of the tube.

fect is due to the unavoidable hypothesis of homogeneous inelastic fields per phase. The issue has been addressed in the literature through proper modifications: the isotropization technique (Chaboche et al., 2005), the linear comparison composite theory accounting for second order moments (Ponte-Castañeda, 1991; Lahellec and Suquet, 2007), or the introduction of a special interphase between the matrix and the reinforcement (Barral et al., 2020). In future works, the developed fully coupled thermomechanical homogenization framework is going to be combined with such techniques.

5. Conclusions and Perspectives

The fully coupled thermomechanical response of composites has been modelled in this work using a mean-field multiscale framework. The connection between macroscopic and microscopic fields and the description of balance and constitutive laws at both scales has been considered to follow the same principles as those described on asymptotic expansion periodic homog-

enization theory (Chatzigeorgiou et al., 2016). The combination of Mori-Tanaka and Transformation Field Analysis, in conjuction to the computation of thermomechanical tangent moduli, has been shown to be an efficient method for the study of composite structures undergoing mechanical and thermal loadings. The numerical examples presented here demonstrate the developed model's accuracy and capabilities.

The designed multiscale framework is capable of analyzing composite materials and their structures with strong influence between thermal and mechanical fields. The last numerical example illustrates the model's capability to simulate cyclic loading conditions on a composite structure, accounting for fully coupled thermomechanical effects. Moreover, the normalization of variables and material properties resolves numerical convergence issues related to the large difference between mechanical and thermal related values of material properties. The temperature variations due to thermoelasticity and dissipation affects the mechanical response, which in turn influences the energy balance. Also, the developed theory can easily integrate other inelastic mechanisms, such as viscoelasticity, damage, or even phase transformation. These phenomena are characterized by strong thermomechanical couplings.

Studying the fatigue life of composites and composite structures under multiple loading cycles is a difficult topic, especially due to the large computational cost. The proposed thermomechanical homogenization framework, combined with cycle jump techniques that reduce the number of cycles at which full computations are required, could be a valuable tool on identifying the fatigue behavior of composite materials and structures (Chen et al., 2023).

In line with the modern needs of the industry for real-time computations, data-driven approaches could be combined with the presented framework. More precisely, one could consider the multiscale framework as a "virtual testing machine" that performs a large number of numerical simulations. The latter could be utilized for the training and testing database of a neural network technique, like FE-MuTINN (El Fallaki Idrissi et al., 2024).

Acknowledgement

The authors acknowledge the use of the Cassiopee Arts et Métiers Institute of Technology HPC Center made available for conducting the research reported in this paper.

References

Alaimo, G., Auricchio, F., Marfia, S., Sacco, E., 2019. Optimization clustering technique for PieceWise Uniform Transformation Field Analysis homogenization of viscoplastic composites. Computational Mechanics 64, 1495–1516. doi:10.1007/s00466-019-01730-2.

Asada, T., Ohno, N., 2007. Fully implicit formulation of elastoplastic homogenization problem for two-scale analysis. International Journal of Solids and Structures 44, 7261–7275. doi:10.1016/j.ijsolstr.2007.04.007.

Barral, M., Chatzigeorgiou, G., Meraghni, F., Léon, R., 2020. Homogenization using modified Mori-Tanaka and TFA framework for elastoplastic-viscoelastic-viscoplastic composites: Theory and numerical validation. International Journal of Plasticity 127, 102632. doi:10.1016/j.ijplas.2019.11.011.

Benaarbia, A., Chatzigeorgiou, G., Kiefer, B., Meraghni, F., 2019. A fully coupled thermo-viscoelastic-viscoplastic-damage framework to study the cyclic variability of the Taylor-Quinney coefficient for semi-crystalline polymers. International Journal of Mechanical Sciences 163, 105128. doi:10.1016/j.ijmecsci.2019.105128.

Benaarbia, A., Chrysochoos, A., Robert, G., 2015. Thermomechanical behavior of PA6.6 composites subjected to low cycle fatigue. Composites Part B: Engineering 76, 52–64. doi:10.1016/j.compositesb.2015.02.011.

Benveniste, Y., 1987. A new approach to the application of Mori-Tanaka's theory in composite materials. Mechanics of Materials 6, 147–157. doi:10.1016/0167-6636(87)90005-6.

Berthelsen, R., Denzer, R., Oppermann, P., Menzel, A., 2017. Computational homogenisation for thermoviscoplasticity: application to thermally sprayed coatings. Computational Mechanics 60, 739–766. doi:10.1007/s00466-017-1436-x.

Boudet, J., Auslender, F., Bornert, M., Lapusta, Y., 2016. An incremental variational formulation for the prediction of the effective work-hardening behavior and field statistics of elasto-(visco)plastic composites. International Journal of Solids and Structures 83, 90–113. doi:10.1016/j.ijsolstr.2016.01.003.

Brassart, L., Stainier, L., Doghri, I., Delannay, L., 2012. Homogenization of elasto-(visco) plastic composites based on an incremental variational

principle. International Journal of Plasticity 36, 86–112. doi:10.1016/j.ijplas.2012.03.010.

Brenner, R., Suquet, P., 2013. Overall response of viscoelastic composites and polycrystals: exact asymptotic relations and approximate estimates. International Journal of Solids and Structures 50, 1824–1838. doi:10.1016/j.ijsolstr.2013.02.011.

Buryachenko, V.A., 2024. Generalized Mori-Tanaka Approach in Peridynamic Micromechanics of Multilayered Composites of Random Structure. Journal of Peridynamics and Nonlocal Modeling in press. doi:10.1007/s42102-023-00114-8.

Cavalcante, M.A.A., Pindera, M.J., 2016. Generalized FVDAM theory for elastic-plastic periodic materials. International Journal of Plasticity 77, 90–117. doi:10.1016/j.ijplas.2015.09.010.

Chaboche, J., Kanoute, P., Ross, A., 2005. On the capabilities of mean-field approaches for the description of plasticity in metal matrix composites. International Journal of Plasticity 21, 1409–1434. doi:10.1016/j.ijplas.2004.07.001.

Charalambakis, N., Chatzigeorgiou, G., Chemisky, Y., Meraghni, F., 2018. Mathematical homogenization of inelastic dissipative materials: A survey and recent progress. Continuum Mechanics and Thermodynamics 30, 1–51. doi:10.1007/s00161-017-0587-5.

Chatzigeorgiou, G., 2022. Study of multilayered composites through periodic

homogenization and Mori-Tanaka methods. Mechanics of Materials 164, 104110. doi:10.1016/j.mechmat.2021.104110.

Chatzigeorgiou, G., Charalambakis, N., Chemisky, Y., Meraghni, F., 2016. Periodic homogenization for fully coupled thermomechanical modeling of dissipative generalized standard materials. International Journal of Plasticity 81, 18–39. doi:10.1016/j.ijplas.2016.01.013.

Chatzigeorgiou, G., Charalambakis, N., Chemisky, Y., Meraghni, F., 2018. Thermomechanical Behavior of Dissipative Composite Materials. ISTE Press - Elsevier, London. doi:10.1016/C2017-0-01481-7.

Chatzigeorgiou, G., Chemisky, Y., Meraghni, F., 2015. Computational micro to macro transitions for shape memory alloy composites using periodic homogenization. Smart Materials and Structures 24, 035009. doi:10.1088/0964-1726/24/3/035009.

Chatzigeorgiou, G., Meraghni, F., 2019. Elastic and inelastic local strain fields in composites with coated fibers or particles: Theory and validation. Mathematics and Mechanics of Solids 24, 2858–2894. doi:10.1177/1081286518822695.

Chatzigeorgiou, G., Meraghni, F., Charalambakis, N., 2022. Multiscale Modeling Approaches for Composites. Elsevier, Amsterdam. doi:10.1016/C2019-0-05214-4.

Chen, Q., Chatzigeorgiou, G., Robert, G., Meraghni, F., 2022. Viscoelastic-Viscoplastic Homogenization of Short Glass-Fiber Reinforced Polyamide Composites (PA66/GF) with Progressive Interphase and Matrix Damage:

New Developments and Experimental Validation. Mechanics of Materials 164, 104081. doi:10.1016/j.mechmat.2021.104081.

Chen, Q., Chatzigeorgiou, G., Robert, G., Meraghni, F., 2023. Combination of mean-field micromechanics and cycle jump technique for cyclic response of PA66/GF composites with viscoelastic-viscoplastic and damage mechanisms. Acta Mechanica 234, 1533–1552. doi:10.1007/s00707-022-03448-4.

Chen, Q., Pindera, M.J., 2020. Homogenization and localization of elastic-plastic nanoporous materials with Gurtin-Murdoch interfaces: An assessment of computational approaches. International Journal of Plasticity 124, 42–70. doi:10.1016/j.ijplas.2019.08.004.

Chen, Q., Wang, G., Chen, X., Geng, J., 2017. Finite-volume homogenization of elastic/viscoelastic periodic materials. Composite Structures 182, 457–470. doi:10.1016/j.compstruct.2017.09.044.

Chrysochoos, A., Huon, V., Jourdan, F., Muracciole, J.M., Peyroux, R., Wattrisse, B., 2010. Use of Full-Field Digital Image Correlation and Infrared Thermography Measurements for the Thermomechanical Analysis of Material Behaviour. Strain 46, 117–130. doi:10.1111/j.1475-1305.2009.00635.x.

Coleman, B.D., Gurtin, M.E., 1967. Thermodynamics with Internal State Variables. The Journal of Chemical Physics 47, 597–613. doi:10.1063/1.1711937.

Covezzi, F. de Miranda, S., Marfia, S., Sacco, E., 2016. Complementary formulation of the TFA for the elasto-plastic analysis of composites. Composite Structures 156, 93–100. doi:10.1016/j.compstruct.2016.01.094.

Czarnota, C., Kowalczyk-Gajewska, K., Salahouelhadj, A., Martiny, M., Mercier, S., 2015. Modeling of the cyclic behavior of elastic-viscoplastic composites by the additive tangent Mori-Tanaka approach and validation by finite element calculations. International Journal of Solids and Structures 56-57, 96–117. doi:10.1016/j.ijsolstr.2014.12.002.

Desrumaux, F., Meraghni, F., Benzeggagh, M.L., 2001. Generalised Mori-Tanaka Scheme to Model Anisotropic Damage Using Numerical Eshelby Tensor. Journal of Composite Materials 35, 603–624. doi:10.1177/002199801772662091.

Doghri, I., Ouaar, A., 2003. Homogenization of two-phase elasto-plastic composite materials and structures: Study of tangent operators, cyclic plasticity and numerical algorithms. International Journal of Solids and Structures 40, 1681–1712. doi:10.1016/S0020-7683(03)00013-1.

Dondeti, P., Paquet, D., Ghosh, S., 2012. A rate-dependent homogenization based continuum plasticity-damage (HCPD) model for dendritic cast aluminum alloys. Engineering Fracture Mechanics 89, 75–97. doi:10.1016/j.engfracmech.2012.04.018.

Dong, H., Zheng, X., Cui, J., Nie, Y., Yang, Z., Yang, Z., 2019. High-order three-scale computational method for dynamic thermo-mechanical problems of composite structures with multiple spatial scales. International

683 Journal of Solids and Structures 169, 95–121. doi:10.1016/j.ijsolstr.
684 2019.04.017.

685 Dvorak, G., 1992. Transformation field analysis of inelastic composite ma-
686 terials. Proceedings of the Royal Society of London A 437, 311–327.
687 doi:10.1098/rspa.1992.0063.

688 Dvorak, G., Benveniste, Y., 1992. On transformation strains and uniform
689 fields in multiphase elastic media. Proceedings of the Royal Society of
690 London A 437, 291–310. doi:10.1098/rspa.1992.0062.

691 El Fallaki Idrissi, M., Praud, F., Meraghni, F., Chinesta, F., Chatzigeor-
692 giou, G., 2024. Multiscale Thermodynamics-Informed Neural Networks
693 (MuTINN) towards fast and frugal inelastic computation of woven com-
694 posite structures. Journal of the Mechanics and Physics of Solids 186,
695 105604. doi:10.1016/j.jmps.2024.105604.

696 Ene, H.I., 1983. On linear thermoelasticity of composite materials. In-
697 ternational Journal of Engineering Science 21, 443–448. doi:10.1016/
698 0020-7225(83)90094-0.

699 Germain, P., 1973. Cours de mécanique des milieux continus, Tome I: Théorie
700 Générale. Masson, Paris.

701 Germain, P., 1982. Sur certaines définitions liées à l'énergie en mécanique des
702 solides. International Journal of Engineering Science 20, 245–259. doi:10.
703 1016/0020-7225(82)90020-9.

704 Germain, P., Nguyen, Q.S., Suquet, P., 1983. Continuum thermodynamics.
705 Journal of Applied Mechanics 50, 1010–1020. doi:10.1115/1.3167184.

Haj-Ali, R., Aboudi, J., 2010. Formulation of the high-fidelity generalized method of cells with arbitrary cell geometry for refined micromechanics and damage in composites. International Journal of Solids and Structures 47, 3447–3461. doi:10.1016/j.ijsolstr.2010.08.022.

Halphen, B., Nguyen, Q.S., 1975. Sur les matériaux standards généralisés. Journal de Mécanique 14, 39–63.

Hatta, H., Taya, M., 1986. Equivalent inclusion method for steady state heat conduction in composites. International Journal of Engineering Science 24, 1159–1172. doi:10.1016/0020-7225(86)90011-X.

Jendli, Z., Meraghni, F., Fitoussi, J., Baptist, D., 2009. Multi-scales modelling of dynamic behaviour for discontinuous fibre SMC composites. Composites Science and Technology 69, 97–103. doi:10.1016/j.compscitech.2007.10.047.

Jiang, T., Shao, J.F., 2009. On the incremental approach for nonlinear homogenization of composite and influence of isotropization. Computational Materials Science 46, 447–451. doi:10.1016/j.commatsci.2009.03.032.

Ju, X., Mahnken, R., Xu, Y., Liang, L., 2022. NTFA-enabled goal-oriented adaptive space-time finite elements for micro-heterogeneous elastoplasticity problems. Computer Methods in Applied Mechanics and Engineering 398, 115199. doi:10.1016/j.cma.2022.115199.

Kotha, S., Ozturk, D., Ghosh, S., 2019. Parametrically homogenized constitutive models (PHCMs) from micromechanical crystal plasticity FE simulations, part I: Sensitivity analysis and parameter identification

for Titanium alloys. International Journal of Plasticity 120, 296–319. doi:10.1016/j.ijplas.2019.05.008.

Kruch, S., Chaboche, J.L., 2011. Multi-scale analysis in elasto-viscoplasticity coupled with damage. International Journal of Plasticity 27, 2026–2039. doi:10.1016/j.ijplas.2011.03.007.

Lahellec, N., Suquet, P., 2007. On the effective behavior of nonlinear inelastic composites: I. Incremental variational principles. Journal of the Mechanics and Physics of Solids 55, 1932–1963. doi:10.1016/j.jmps.2007.02.003.

Lahellec, N., Suquet, P., 2013. Effective response and field statistics in elasto-plastic and elasto-viscoplastic composites under radial and non-radial loadings. International Journal of Plasticity 42, 1–30. doi:10.1016/j.ijplas.2012.09.005.

Lemaitre, J., Chaboche, J.L., 2002. Mechanics of solid materials. Cambridge University Press, Cambridge. doi:10.1017/CBO9781139167970.

Li, J., Romero, I., Segurado, J., 2019. Development of a thermo-mechanically coupled crystal plasticity modeling framework: Application to polycrystalline homogenization. International Journal of Plasticity 119, 313–330. doi:10.1016/j.ijplas.2019.04.008.

Lubliner, J., 1972. On the thermodynamic foundations of non-linear solid mechanics. International Journal of Non-Linear Mechanics 7, 237–254. doi:10.1016/0020-7462(72)90048-0.

Meraghni, F., Desrumaux, F., Benzeggagh, M.L., 2002. Implementation of a constitutive micromechanical model for damage analysis in glass mat

reinforced composite structures. Composites Science and Technology 62, 2087–2097. doi:10.1016/S0266-3538(02)00110-0.

Mercier, S., Molinari, A., 2009. Homogenization of elastic-viscoplastic heterogeneous materials: Self-consistent and Mori-Tanaka schemes. International Journal of Plasticity 25, 1024–1048. doi:10.1016/j.ijplas.2008.08.006.

Michel, J.C., Moulinec, H., Suquet, P., 1999. Effective properties of composite materials with periodic microstructure: a computational approach. Computer Methods in Applied Mechanics and Engineering 172, 109–143. doi:10.1016/S0045-7825(98)00227-8.

Michel, J.C., Suquet, P., 2004. Computational analysis of nonlinear composites structures using the nonuniform transformation field analysis. Computer Methods in Applied Mechanics and Engineering 193, 5477–5502. doi:10.1016/j.cma.2003.12.071.

Miled, B., Doghri, I., Brassart, L., Delannay, L., 2013. Micromechanical modeling of coupled viscoelastic-viscoplastic composites based on an incrementally affine formulation. International Journal of Solids and Structures 50, 1755–1769. doi:10.1016/j.ijsolstr.2013.02.004.

Mori, T., Tanaka, K., 1973. Average stress in matrix and average elastic energy of materials with misfitting inclusions. Acta Metallurgica 21, 571–574. doi:10.1016/0001-6160(73)90064-3.

Nachtane, M., Meraghni, F., Chatzigeorgiou, G., Harper, L.T., Pelascini, F., 2022. Multiscale viscoplastic modeling of recycled glass fiber-reinforced thermoplastic composites: Experimental and numerical inves-

tigations. Composites Part B: Engineering 242, 110087. doi:10.1016/j.compositesb.2022.110087.

Onimus, F., Gelebart, L., Brenner, R., 2022. Polycrystalline simulations of in-reactor deformation of recrystallized Zircaloy-4 tubes: Fast Fourier Transform computations and mean-field self-consistent model. International Journal of Plasticity 153, 103272. doi:10.1016/j.ijplas.2022.103272.

Ponte-Castañeda, P., 1991. The effective mechanical properties of nonlinear isotropic composites. Journal of the Mechanics and Physics of Solids 39, 45–71. doi:10.1016/0022-5096(91)90030-R.

Praud, F., Chatzigeorgiou, G., Meraghni, F., 2021. Fully integrated multi-scale modelling of damage and time-dependency in thermoplastic-based woven composites. International Journal of Damage Mechanics 30, 163–195. doi:10.1177/1056789520944986.

Rao, W., Zhang, J., Kang, G., Yu, C., Jiang, H., 2019. A meso-mechanical constitutive model of bulk metallic glass composites considering the local failure of matrix. International Journal of Plasticity 115, 238–267. doi:10.1016/j.ijplas.2018.11.017.

Schneider, M., 2017. An FFT-based fast gradient method for elastic and inelastic unit cell homogenization problems. Computer Methods in Applied Mechanics and Engineering 315, 846–866. doi:10.1016/j.cma.2016.11.004.

Schneider, M., 2021. A review of nonlinear FFT-based computational homog-

enization methods. Review and Perspective in Mechanics 232, 2051–2100. doi:10.1007/s00707-021-02962-1.

Schöneich, M., Dinzart, F., Sabar, H., Berbenni, S., Stommel, M., 2017. A coated inclusion-based homogenization scheme for viscoelastic composites with interphases. Mechanics of Materials 105, 89–98. doi:10.1016/j.mechmat.2016.11.009.

Sengupta, A., Papadopoulos, P., Taylor, R.L., 2012. A multiscale finite element method for modeling fully coupled thermomechanical problems in solids. International Journal for Numerical Methods in Engineering 91, 1386–1405. doi:10.1002/nme.4320.

Simo, J.C., Hughes, T.J.R., 1998. Computational Inelasticity. Springer-Verlag, New York. doi:10.1007/b98904.

Temizer, I., 2012. On the asymptotic expansion treatment of two-scale finite thermoelasticity. International Journal of Engineering Science 53, 74–84. doi:10.1016/j.ijengsci.2012.01.003.

Terada, K., Kikuchi, N., 2001. A class of general algorithms for multi-scale analyses of heterogeneous media. Computer Methods in Applied Mechanics and Engineering 190, 5427–5464. doi:10.1016/S0045-7825(01)00179-7.

Tikarrouchine, E., Benaarbia, A., Chatzigeorgiou, G., Meraghni, F., 2021. Non-linear FE^2 multiscale simulation of damage, micro and macroscopic strains in polyamide 66-woven composite structures: analysis and experimental validation. Composite Structures 255, 112926. doi:10.1016/j.compstruct.2020.112926.

Tikarrouchine, E., Chatzigeorgiou, G., Chemisky, Y., Meraghni, F., 2019. Fully coupled thermo-viscoplastic analysis of composite structures by means of multi-scale three-dimensional finite element computations. International Journal of Solids and Structures 164, 120–140. doi:10.1016/j.ijsolstr.2019.01.018.

Tu, W., Pindera, M.J., 2016. Damage evolution in cross-ply laminates revisited via cohesive zone model and finite-volume homogenization. Composites Part B: Engineering 86, 40–60. doi:10.1016/j.compositesb.2015.09.039.

Vu, Q.H., Brenner, R., Castelnau, O., Moulinec, H., Suquet, P., 2012. A self-consistent estimate for linear viscoelastic polycrystals with internal variables inferred from the collocation method. Modelling and Simulation in Materials Science and Engineering 20, 024003. doi:10.1088/0965-0393/20/2/024003.

Wicht, D., Schneider, M., Böhlke, T., 2021. Computing the effective response of heterogeneous materials with thermomechanically coupled constituents by an implicit fast Fourier transform-based approach. International Journal for Numerical Methods in Engineering 122, 1307–1332. doi:10.1002/nme.6579.

Wright, T.W., 2002. The physics and mathematics of adiabatic shear bands. Cambridge University Press, Cambridge.

Wu, L., Adam, L., Doghri, I., Noels, L., 2017. An incremental-secant mean-field homogenization method with second statistical moments for elasto-

visco-plastic composite materials. Mechanics of Materials 114, 180–200. doi:10.1016/j.mechmat.2017.08.006.

Wu, L., Noels, L., Adam, L., Doghri, I., 2013. An implicit-gradient-enhanced incremental-secant mean-field homogenization scheme for elasto-plastic composites with damage. International Journal of Solids and Structures 50, 3843–3860. doi:10.1016/j.ijsolstr.2013.07.022.

Yang, Z., Liu, Y., Sun, Y., Jing, Y., Ma, Q., 2020. A novel second-order reduced homogenization approach for nonlinear thermo-mechanical problems of axisymmetric structures with periodic micro-configurations. Computer Methods in Applied Mechanics and Engineering 368, 113126. doi:10.1016/j.cma.2020.113126.

Yu, Q., Fish, J., 2002. Multiscale asymptotic homogenization for multi-physics problems with multiple spatial and temporal scales: a coupled thermo-viscoelastic example problem. International Journal of Solids and Structures 39, 6429–6452. doi:10.1016/S0020-7683(02)00255-X.

Yun, G.J., Zhu, F.Y., Lim, H.J., Choi, H., 2021. A damage plasticity constitutive model for wavy CNT nanocomposites by incremental Mori-Tanaka approach. Composite Structures 258, 113178. doi:10.1016/j.compstruct.2020.113178.

Zecevic, M., Knezevic, M., 2018. Latent hardening within the elasto-plastic self-consistent polycrystal homogenization to enable the prediction of anisotropy of AA6022-T4 sheets. International Journal of Plasticity 105, 141–163. doi:10.1016/j.ijplas.2018.02.007.

Appendix A. Normalization of thermomechanical problem

Let's consider a thermoelastic-thermoviscoplastic body. The 3-D thermo-mechanical problem is expressed by the following kinematics and conservation laws,

$$\begin{aligned} \varepsilon_{ij} &= \frac{1}{2}\frac{\partial u_i}{\partial x_j} + \frac{1}{2}\frac{\partial u_j}{\partial x_i}, \\ \frac{\partial \sigma_{ij}}{\partial x_j} &= 0, \\ -\frac{\partial q_i}{\partial x_i} &= -r, \end{aligned} \tag{A.1}$$

accompanied by the constitutive relations

$$\begin{aligned} \sigma_{ij} &= C_{ijkl}\left[\varepsilon_{kl} - \varepsilon^p_{kl} - \alpha_{kl}[\theta - \theta_{\mathrm{ref}}]\right], \\ \frac{\mathrm{d}\varepsilon^p_{kl}}{\mathrm{d}t} &= \frac{3\sigma'_{ij}}{2\sigma^{\mathrm{VM}}}\frac{\mathrm{d}p}{\mathrm{d}t}, \\ \sigma'_{ij} &= \sigma_{ij} - \sigma_{kk}\delta_{ij}, \quad \sigma^{\mathrm{VM}} = \sqrt{\frac{3}{2}\sigma'_{ij}\sigma'_{ij}}, \end{aligned} \tag{A.2}$$

$$\begin{aligned} F &= Q_1 p + Q_2[1 - \exp(-bp)], \\ W(\theta) &= \exp(-\theta_v/\theta), \\ \frac{\mathrm{d}p}{\mathrm{d}t} &= \begin{cases} 0, & \sigma^{\mathrm{vM}} - Y - F < 0, \\ \left[\dfrac{\sigma^{\mathrm{vM}} - Y - F}{K_a}\right]^{N_a} W(\theta), & \sigma^{\mathrm{vM}} - Y - F \geqslant 0, \end{cases} \end{aligned} \tag{A.3}$$

$$\begin{aligned} \gamma_{\mathrm{loc}} &= \sigma_{ij}\frac{\mathrm{d}\varepsilon^p_{ij}}{\mathrm{d}t} - F\frac{\mathrm{d}p}{\mathrm{d}t}, \\ r &= -\rho c\frac{\mathrm{d}\theta}{\mathrm{d}t} - \theta\alpha_{ij}\frac{\mathrm{d}\sigma_{ij}}{\mathrm{d}t} + \gamma_{\mathrm{loc}}, \\ q_i &= -\kappa_{ij}\frac{\partial\theta}{\partial x_j}. \end{aligned} \tag{A.4}$$

In the above expressions δ_{ij} is the Kronecker delta. The material parameters Y, Q_1, Q_2, b, K_a and N_a are related to the viscoplastic behavior. $W(\theta)$ denotes an Maxwell probability law function and θ_v is the related material parameter. The body forces and the heat sources are neglected for simplicity.

Following Wright (2002), the real time and space are substituted by their normalized counterparts. Also, the stress tensor and the product of density and specific heat capacity are substituted by unitless quantities. Thus, the following relations are assumed:

$$\tau = \dot{\gamma}_0 t, \quad y_i = \frac{x_i}{H}, \quad s_{ij} = \frac{\sigma_{ij}}{s_0}, \quad \omega = \frac{\rho c}{\rho_0 c_0}, \tag{A.5}$$

where H is a space dimension (usually equal to the maximum length of the structure), $\dot{\gamma}_0$ is related to the strain rate loading, s_0 is a stress type predefined quantity and $\rho_0 c_0$ is a fixed product of density and specific heat capacity. The expressions (A.5) lead to the normalized variables

$$\begin{aligned} v_i &= \frac{u_i}{H}, & \vartheta &= \frac{\rho_0 c_0 \theta}{s_0}, \\ \mathtt{q}_i &= \frac{q_i}{s_0 \dot{\gamma}_0 H}, & g_{\mathrm{loc}} &= \frac{\gamma_{\mathrm{loc}}}{s_0 \dot{\gamma}_0}, \\ \mathtt{r} &= \frac{r}{s_0 \dot{\gamma}_0}, \end{aligned} \tag{A.6}$$

and the normalized parameters

$$\begin{aligned} \mathtt{C}_{ijkl} &= \frac{C_{ijkl}}{s_0}, & \vartheta_{\mathrm{ref}} &= \frac{\rho_0 c_0 \theta_{\mathrm{ref}}}{s_0}, \\ k_{ij} &= \frac{\kappa_{ij}}{\rho_0 c_0 \dot{\gamma}_0 H^2}, & a_{ij} &= \frac{s_0 \alpha_{ij}}{\rho_0 c_0}, \\ \mathtt{Y} &= \frac{Y}{s_0}, & \mathtt{K}_a &= \frac{K_a}{s_0} [\dot{\gamma}_0]^{1/N_a}, \\ \mathtt{Q}_1 &= \frac{Q_1}{s_0}, & \mathtt{Q}_2 &= \frac{Q_2}{s_0}, \\ \vartheta_v &= \frac{\rho_0 c_0 \theta_v}{s_0}. \end{aligned} \tag{A.7}$$

Accordingly, the time and spatial derivatives are expressed as

$$\frac{\mathrm{d}}{\mathrm{d}t} = \dot{\gamma}_0 \frac{\mathrm{d}}{\mathrm{d}\tau}, \qquad \frac{\partial}{\partial x} = \frac{1}{H}\frac{\partial}{\partial y}.$$

Considering the above, the initial system (A.1)-(A.4) takes the normalized form

$$\begin{aligned} \varepsilon_{ij} &= \frac{1}{2}\frac{\partial v_i}{\partial y_j} + \frac{1}{2}\frac{\partial v_j}{\partial y_i}, \\ \frac{\partial s_{ij}}{\partial y_j} &= 0, \\ -\frac{\partial \mathtt{q}_i}{\partial y_i} &= -\mathtt{r}, \end{aligned} \tag{A.8}$$

and

$$\begin{aligned} s_{ij} &= \mathtt{C}_{ijkl}\left[\varepsilon_{kl} - \varepsilon^p_{kl} - a_{kl}[\vartheta - \vartheta_{\mathrm{ref}}]\right], \\ \frac{\mathrm{d}\varepsilon^p_{kl}}{\mathrm{d}\tau} &= \frac{3 s'_{ij}}{2 s^{\mathrm{VM}}}\frac{\mathrm{d}p}{\mathrm{d}\tau}, \\ s'_{ij} &= s_{ij} - s_{kk}\delta_{ij}, \quad s^{\mathrm{VM}} = \sqrt{\frac{3}{2} s'_{ij} s'_{ij}}, \end{aligned} \tag{A.9}$$

$$\begin{aligned} \mathtt{F} &= \mathtt{Q}_1 p + \mathtt{Q}_2[1 - \exp(-bp)], \\ \mathtt{W}(\vartheta) &= \exp\left(-\vartheta_v/\vartheta\right), \\ \frac{\mathrm{d}p}{\mathrm{d}\tau} &= \begin{cases} 0, & s^{\mathrm{VM}} - \mathtt{Y} - \mathtt{F} < 0, \\ \left[\dfrac{s^{\mathrm{VM}} - \mathtt{Y} - \mathtt{F}}{\mathtt{K}_a}\right]^{N_a} \mathtt{W}(\vartheta), & s^{\mathrm{VM}} - \mathtt{Y} - \mathtt{F} \geqslant 0, \end{cases} \end{aligned} \tag{A.10}$$

$$\begin{aligned} g_{\mathrm{loc}} &= s_{ij}\frac{\mathrm{d}\varepsilon^p_{ij}}{\mathrm{d}\tau} - \mathtt{F}\frac{\mathrm{d}p}{\mathrm{d}\tau}, \\ \mathtt{r} &= -\omega\frac{\mathrm{d}\vartheta}{\mathrm{d}\tau} - \vartheta a_{ij}\frac{\mathrm{d}s_{ij}}{\mathrm{d}\tau} + g_{\mathrm{loc}}, \\ \mathtt{q}_i &= -k_{ij}\frac{\partial \vartheta}{\partial y_j}. \end{aligned} \tag{A.11}$$

For the example of subsection 4.2, the normalized material properties of the constituents and the normalized thermal conductivities of the overall composite are provided in Tables A.1 and A.2 respectively. The corresponding quantities for the example of subsection 4.3 are shown in Tables A.3 and A.4.

property	glass	epoxy
$\mathtt{E}$	1	0.0416667
ν	0.22	0.3
a	0.2252	4.1284
ω	1.0425	0.9575
k	0.417	0.1668
$\mathtt{Y}$		$6.6667 \cdot 10^{-4}$
$\mathtt{K}_a$		$6.9444 \cdot 10^{-5}$
N_a		5
$\mathtt{Q}_1$		$1.3889 \cdot 10^{-3}$
$\mathtt{Q}_2$		$1.3889 \cdot 10^{-4}$
b		5

Table A.1: Normalized thermomechanical properties of constituents in the example of subsection 4.2. Since the viscoplastic criterion is temperature independent, $\theta_v = 0$.

property	epoxy based composite
k_{11}	0.2383
k_{22}	0.2919
k_{33}	0.2919

Table A.2: Normalized thermal conductivity of the homogenized medium (epoxy based composite) in the example of subsection 4.2.

property	glass	PA66
$\mathtt{E}$	1	0.0416667
ν	0.22	0.3
a	0.2252	4.1284
ω	1.0425	0.9575
k	0.417	0.1668
$\mathtt{Y}$		$1.3889 \cdot 10^{-5}$
$\mathtt{K}_a$		$1.4093 \cdot 10^{-5}$
N_a		2.37
$\mathtt{Q}_1$		$3.6111 \cdot 10^{-3}$
$\mathtt{Q}_2$		$5.4167 \cdot 10^{-4}$
b		134
ϑ_v		$7.811 \cdot 10^{-4}$

Table A.3: Normalized thermomechanical properties of constituents in the example of subsection 4.3.

property	PA66 based composite
k_{11}	0.2578
k_{22}	0.2578
k_{33}	0.2919

Table A.4: Normalized thermal conductivity of the homogenized medium (PA66 based composite) in the example of subsection 4.3.

Appendix B. Tangent moduli of a thermoviscoplastic material

For a thermoviscoplastic material whose constitutive law is expressed through the equations (A.2), (A.3), (A.4), the thermomechanical tangent moduli can be estimated using the return mapping algorithm/convex cutting plane technique. Analytical details for obtaining them can be found in Chatzigeorgiou et al. (2018). Here, only the final formulas are given.

Before presenting the formulas, it is worth mentioning that: i) the superscript (n) denotes the value of a variable at the time step n, and ii) $\Delta\{\bullet\}$ denotes the difference of the values of the variable $\{\bullet\}$ between the time steps $n+1$ and n.

The required tangent moduli for the thermomechanical analyses are given by the expressions

$$\begin{aligned}
\boldsymbol{D}^{\varepsilon} &= \boldsymbol{C} - [\boldsymbol{C}:\boldsymbol{\Lambda}_p] \otimes \boldsymbol{P}^{\varepsilon}, \\
\boldsymbol{D}^{\theta} &= -\boldsymbol{C}:\boldsymbol{\alpha} - \boldsymbol{C}:\boldsymbol{\Lambda}_p P^{\theta}, \\
\boldsymbol{R}^{\varepsilon} &= -\frac{\theta}{\Delta t}\boldsymbol{\alpha}:\boldsymbol{D}^{\varepsilon} + \frac{1}{\Delta t}\boldsymbol{\Gamma}^{\varepsilon}, \\
R^{\theta} &= -\frac{1}{\Delta t}\left[c_0 + c_0 \ln\left(\frac{\theta}{\theta^{(n)}}\right) + \boldsymbol{\alpha}:\Delta\boldsymbol{\sigma} + \theta\boldsymbol{\alpha}:\boldsymbol{D}^{\theta}\right] + \frac{1}{\Delta t}\Gamma^{\theta},
\end{aligned}$$

where

$$\begin{aligned}
\boldsymbol{P}^{\varepsilon} &= \frac{\Omega}{\omega}\boldsymbol{\Lambda}_p:\boldsymbol{C}, \\
P^{\theta} &= -\frac{1}{\omega}\left[\Omega\boldsymbol{\Lambda}_p:\boldsymbol{C}:\boldsymbol{\alpha} - \Omega^{*}\right], \\
\boldsymbol{\Gamma}^{\varepsilon} &= \Delta p\boldsymbol{\Lambda}_p:\boldsymbol{D}^{\varepsilon} + \left[\sigma^{VM} - F - \Delta p\frac{\mathrm{d}F}{\mathrm{d}p}\right]\boldsymbol{P}^{\varepsilon}, \\
\Gamma^{\theta} &= \Delta p\boldsymbol{\Lambda}_p:\boldsymbol{D}^{\theta} + \left[\sigma^{VM} - F - \Delta p\frac{\mathrm{d}F}{\mathrm{d}p}\right]P^{\theta},
\end{aligned}$$

and

$$
\begin{aligned}
\boldsymbol{\Lambda}_p &= \frac{3\boldsymbol{\sigma}'}{2\sigma^{VM}}, \\
\Omega &= \frac{N_a}{2K_a}\left[\frac{\langle\Phi\rangle_+}{K_a}\right]^{N_a-1}\left[1+\frac{\Phi}{|\Phi|}\right]W(\theta), \\
\Omega^* &= \left[\frac{\langle\Phi\rangle_+}{K_a}\right]^{N_a}\frac{\theta_v}{\theta^2}W(\theta), \\
\omega &= \Omega\left[\boldsymbol{\Lambda}_p : \boldsymbol{C} : \boldsymbol{\Lambda}_p + \frac{\mathrm{d}F}{\mathrm{d}p}\right] + \frac{1}{\Delta t}, \\
\Phi &= \sigma^{VM} - F - Y.
\end{aligned}
$$

The material parameters and several functions and variables are discussed in Appendix A and in the main text.

Highlights

- The proposed thermomechanical homogenization framework combines Mori-Tanaka and TFA.
- Fully coupled thermomechanical modeling for viscoplastic dissipative mechanism.
- Balance and constitutive laws are accounted for in micro- and macroscopic scales.
- Concentration tensors are computed for evaluating thermomechanical tangent moduli.
- FE implementation in full-structure analysis to show the framework's capabilities.

Declaration of Interest Statement

Authors: G. Chatzigeorgiou, F. Meraghni, Q. Chen:
Manuscript title: Fully coupled nonlinear thermomechanical modeling of composites using mean-field Mori-Tanaka scheme combined with TFA theory

The authors declare that they have no known competing financial interests or personal relationships that could have appeared to influence the work reported in this article.

Metz, November 6, 2023